Simulation of IP_3 receptor function in cerebellar Purkinje cell dendritic spine: Importance of stochasticity

MASTER'S THESIS

Katri Hituri
Institute of Medical Technology
University of Tampere

May 2007

Preface

This Master's thesis was done in the Institute of Medical Technology at the University of Tampere. The practical work was carried out in the Theoretical Neurobiology Laboratory at the University of Antwerp in Belgium and in the Computational Neuroscience research group (CNS) in the Institute of Signal Processing at Tampere University of Technology (TUT).

First, I want to acknowledge my supervisors Academy Research Fellow Marja-Leena Linne and Dr. Pablo Achard for their excellent guidance, advice, and support during this work. I am also grateful to Prof. Erik De Schutter for the opportunity to work in his research group in Belgium, and to Stefan Wils, M.Sc., for his guidance in practical work. I thank Tiina Manninen, M.Sc., for help with the mathematical notations and also my other co-workers at TUT. This work was supported by the Academy of Finland (application number 213462, Finnish Programme for Centres of Excellence in Research 2006-2011). The Finnish Cultural Foundation is also acknowledged for financial support. I thank warmly Ms. Isabella Wierinckx and Ms. Evelyne Justens for their hospitality and making my visit in Belgium pleasant and rewarding. Finally, I would like to express my gratitude to my family, Mika Holm, and friends for their support.

May 2007, Tampere

Katri Hituri

MASTER'S THESIS

Place:	UNIVERSITY OF TAMPERE Faculty of Medicine, Institute of Medical Technology
Author:	HITURI, KATRI SUVI-PÄIVIKKI
Title:	Simulation of IP_3 receptor function in cerebellar Purkinje cell dendritic spine: Importance of stochasticity
Pages:	61 pp. + appendix 6 pp.
Supervisors:	Academy Research Fellow Marja-Leena Linne, Ph.D. Senior Researcher Pablo Achard, Ph.D.
Reviewers:	Prof. Markku Kulomaa, Academy Research Fellow Marja-Leena Linne
Date:	May 2007

Abstract

Background and aims: This thesis investigates calcium dynamics in cerebellar Purkinje cells. A special emphasis is put on the Purkinje cells dendritic spines where most of the synapses are formed. Transient rises in cytosolic calcium concentration in spines have a crucial role in initiating long-term depression (LTD) of synaptic activity. LTD is one form of synaptic plasticity and it has been found to be one of the mechanisms of motor learning. One of the most important factors in calcium dynamics is the inositol-1,4,5-trisphosphate receptor (IP_3 receptor). This protein is a ligand binding calcium channel and it is responsible for releasing calcium from endoplasmic reticulum to cytosol. The IP_3 receptor is highly expressed in Purkinje cell spines. Modeling and simulation are an effective way to study the dynamics of intracellular events. The small volume of the spine increases the stochasticity (randomness) in the biochemical processes and this aspect is not considered in traditional deterministic simulations. In this study, the importance of stochasticity in simulation of the function of IP_3 receptor was examined. Stochastic simulations are assumed to produce more realistic results compared to deterministic simulations. The aim of my research was to study the effect of stochasticity in modeling by comparing stochastic and deterministic simulations of the function of IP_3 receptor, located in cerebellar Purkinje cell dendritic spine.

Methods: Based on a large literature review, two different mathematical models describing the function of IP_3 receptor were chosen as test cases. In short, both models describe the reaction kinetics of IP_3 receptor. These models were simulated both on a deterministic simulator and on a more biologically correct stochastic simulator. Two different kinds of simulations, open probability and dynamic, were performed with both simulators.

Results: For both models, open probability simulations produced similar results with deterministic and stochastic simulators. In dynamic simulations the time evolution of cytosolic calcium concentration was examined. For small calcium concentrations, there was a significant difference between deterministic and stochastic simulation results.

Conclusions: Results of the open-probability simulations verified that the models were implemented correctly. It can be shown based on dynamic simulation results, that there exists a threshold below which the effect of stochasticity in reaction kinetics becomes meaningful. In conclusion, the deterministic simulations do not produce biologically realistic results under all conditions.

PRO GRADU -TUTKIELMA

Paikka:	TAMPEREEN YLIOPISTO Lääketieteellinen tiedekunta, Lääketieteellisen teknologian instituutti
Tekijä:	HITURI, KATRI SUVI-PÄIVIKKI
Otsikko:	Simulaatiotutkimus satunnaisuuden merkityksestä IP_3-reseptorin toiminnassa pikkuaivojen Purkinje-solussa
Sivumäärä:	61 s. + liite 6 s.
Ohjaajat:	Akatemiatutkija, TkT Marja-Leena Linne Vanhempi tutkija, Ph.D. Pablo Achard
Tarkastajat:	prof. Markku Kulomaa, akatemiatutkija Marja-Leena Linne
Päiväys:	Toukokuu 2007

Tiivistelmä

Tutkimuksen tausta ja tavoitteet: Tässä työssä tutkitaan kalsiumdynamiikkaa pikkuaivojen Purkinje-soluissa. Erityisenä tarkastelun kohteena ovat Purkinje-solun dendriittien pienet ulokkeet, joihin dendriittien synapsit pääasiallisesti muodostuvat. Väliaikaisilla kalsiumpitoisuuden nousuilla on tärkeä rooli pitkäaikaisen synaptisen aktiivisuuden alenemisessa (engl. long-term depression, LTD). LTD on yksi synaptisen muovautuvuuden (engl. synaptic plasticity) muodoista, ja sen on todettu olevan yksi tärkeimmistä motorisen oppimisen mekanismeista. Yksi merkittävimmistä osatekijöistä kalsiumdynamiikassa on inositoli-1,4,5-trisfosfaattireseptori (IP_3-reseptori). Tämä kalvoproteiini muodostaa kanavan, joka vapauttaa avautuessaan kalsiumia solun sisäisestä varastosta. IP_3-reseptoreita on runsaasti Purkinje-solun ulokkeissa. Solussa tapahtuvaa dynaamista toimintaa voidaan tutkia tehokkaasti matemaattisten mallien ja simuloinnin avulla. Koska dendriittien ulokkeiden tilavuus on pieni, satunnaisuus siellä tapahtuvissa prosesseissa lisääntyy, eikä satunnaisuutta ole otettu huomioon perinteisissä deterministisesti toteutetuissa simulaatioissa. Tässä työssä tutkittiin tietynlaisen satunnaisuuden eli stokastisuuden merkitystä IP_3-reseptorin toiminnan simuloinnissa. Stokastisilla simulaatioilla saadaan biologisesti todenmukaisempia tuloksia kuin deterministisillä simulaatioilla. Tutkimuksen tarkoituksena oli selvittää stokastisuuden merkitystä IP_3-reseptorin toiminnan mallinnuksessa ja simuloinnissa pikkuaivojen Purkinje-solujen dendriittien ulokkeissa.

Tutkimusmenetelmät: Työssä käytettiin kahta erilaista IP_3-reseptorin toimintaa kuvaavaa matemaattista mallia. Molempia malleja simuloitiin sekä tavallisella deterministisellä että biologisesti todenmukaisemmalla stokastisella simulaatio-ohjelmalla. Simulaatioita tehtiin molemmilla ohjelmilla kahdenlaisia: reseptorin aukiolotodennäköisyyden ja dynaamisen toiminnan simulaatioita.

Tutkimustulokset: Aukiolotodennäköisyyttä mallintavien simulaatioiden tulokset olivat samanlaisia deterministisellä ja stokastisella simulaatio-ohjelmalla molempien mallien kohdalla. Dynaamisissa simulaatioissa seurattiin kalsiumkonsentraatiota ajan funktiona. Näissä simulaatioissa havaittiin eroa deterministisen ja stokastisten simulaatiotulosten välillä pienillä kalsiumin konsentraatioarvoilla.

Johtopäätökset: Aukiolotodennäköisyyssimulaatioiden tulokset osoittivat, että käytetyt mallit toimivat simulaattoreissa oikein. Dynaamisten simulaatioiden tulosten perusteella voidaan päätellä, että ainakin IP_3-reseptorin kohdalla on olemassa raja-arvo, jonka alapuolella stokastisuuden vaikutus reaktiokinetiikassa on merkittävä. Deterministiset simulaatiot eivät tuota kaikissa olosuhteissa biologisesti todenmukaisia tuloksia.

Contents

Abbreviations and symbols

δ2R	δ2 receptor
AA	arachidonic acid
AMPA	α-amino-3-hydroxy-5-methylisoxazole-4-propionic acid
AMPAR	AMPA receptor
ATP	adenosine triphosphate
BNDF	brain-derived neurotrophic factor
Ca^{2+}	calcium ion
CF	climbing fiber
cGMP	cyclic GMP
CME	chemical master equation
CPU	central processing unit (in computer)
CRF	corticotropin-releasing factor
CRFR1	CRF type 1 receptor
DAG	diacylglycerol
EPSC	excitatory postsynaptic current (causes EPSP)
EPSP	excitatory postsynaptic potential
ER	endoplasmic reticulum
GABA	γ-aminobutyric acid
GC	guanylyl cyclase
Glu	glutamate
GMP	guanosine monophosphate
IGF1	insulin-like growth factor 1
IP_3	inositol-1,4,5-trisphosphate
IP_3R	inositol-1,4,5-trisphosphate receptor
IP_3R1	type 1 inositol-1,4,5-trisphosphate receptor
K^+	potassium ion
LTD	long-term depression
mGluR1	type 1 metabotropic glutamate receptor
IGF1R	IGF1 receptor
MAPK	mitogen-activated protein kinase
MEK	MAPK kinase
MF	mossy fiber
Na^+	sodium ion
Na^+/Ca^{2+}	Na^+-driven Ca^{2+} exchanger
NO	nitric oxide
NMDA	N-methyl-D-aspartate
NMDAR	NMDA receptor
ODE	ordinary differential equation
PF	parallel fiber
PIP_2	phosphatidylinositol 4,5-bisphosphate
PKC	protein kinase C
PKG	protein kinase G
PLA_2	phospholipase A_2
PLC	phospholipase C
PMCA	plasma membrane Ca^{2+}-ATPase
PP2A	protein phosphatase 2A
PSD	postsynaptic density

PTK	protein tyrosine kinase
RyR	ryanodine receptor
SER	smooth endoplasmic reticulum
SERCA	sarcoplasmic/endoplasmic reticulum calcium ATPase
SG	slow-EPSP generator associated with mGluR1
SSA	Gillespie stochastic simulation algorithm
VGCC	voltage-gated Ca^{2+} channel

[A]	concentration of substance A
Da	dalton, unit of molecular mass
M	molarity, mol/l

1 Introduction

It is known that transient rises in the cytosolic calcium (Ca^{2+}) concentration have an important functional role in neurons. In cerebellar Purkinje cell dendritic spines, they have a major role in generation of long-term depression (LTD) of synaptic strength (Konnerth et al., 1992; Ito, 2001). These temporary rises are due to the Ca^{2+} entry from the extracellular space and Ca^{2+} release from intracellular stores such as endoplasmic reticulum (ER). In Purkinje cell spines, inositol-1,4,5-trisphosphate (IP_3) receptors (IP_3Rs) are responsible for Ca^{2+} release from ER. IP_3 receptors are relatively highly expressed in spines (Maeda et al., 1989; Sharp et al., 1999) and essential for LTD induction (Ito, 2001). It has been experimentally shown that IP_3-mediated Ca^{2+} release in spines is a key mediator of LTD (Miyata et al., 2000; Sabatini et al., 2001).

Mathematical modeling is one of the important tools when trying to understand the complex behavior of proteins and other molecules in addition to the networks and pathways they are involved with. Several models have been proposed to describe the behavior of IP_3 receptor (for a comprehensive review see, for example, Sneyd and Falcke, 2005). All the IP_3 receptor models and simulations have been deterministic until the recent years. Deterministic models show the average behavior of the system, i.e. not include any kind of randomness. However, when biochemical reactions occur in very small volumes, such as in dendritic spines, the number of molecules is low even with fairly large concentrations. The small number of molecules increases the possibilities for stochasticity of biochemical reactions and both the randomness of molecular encounters and the fluctuations in the transitions between the conformational states of proteins become functionally relevant. Because of the small volume of the Purkinje cell spine, it is of interest to test the stochastic nature of the system and to take the stochasticity into account in simulations to obtain biologically realistic results. Even though the deterministic approach is adequate in some cases, it thus does not reflect the detailed nature of the biological system (Turner et al., 2004).

The aim of this work was to study the effects of stochasticity on IP_3 receptor functioning and Ca^{2+} dynamics in Purkinje cell spines. Among many mathematical

models of IP_3 receptor functioning two were chosen as test cases. The selected models were implemented into two different simulators: GENESIS/Kinetikit (Bower and Beeman, 1998; Bhalla and Iyengar, 1999; Bhalla, 2002) for deterministic simulations and STEPS (Wils and De Schutter, 2005; Wils and De Schutter, 2006) for stochastic simulations. Two types of different simulations, open probability simulations and dynamic simulations were done for the models with both deterministic and stochastic simulation approaches. The results obtained from stochastic simulations were compared with those obtained from deterministic simulations.

This work has been presented as a poster at the 15th Annual Meeting of the Organization for Computational Neurosciences CNS*2006 (Hituri et al., 2006).

2 Review of literature

2.1 Cerebellum

2.1.1 Structure and functional role

The cerebellum is a part of the brain located beneath the cerebrum at the back of the head. It consists of several different sections, but it can be roughly divided into two hemispheres and a central part (*vermis*). The cerebellum has outer gray matter (cerebellar cortex) and inner white matter like the cerebrum. It occupies about 10 % of the total volume of the brain but contains more than half of all its neurons. Neurons of the cerebellum are highly organized forming separate similar structural units or circuit modules (Bloedel, 1992). Despite this, the cerebellum is divided into several functional regions which make connections with different parts of the brain (Ghez and Thach, 2000).

The cerebellum can be anatomically divided into 20 different lobules, ten in the *vermis* (I-X) and ten in the hemispheres (HI-HX), and also functionally into seven mediolaterally parallel longitudinal zones (A, B, C1, C2, C3, D1, D2) (Ito, 2006). These zones are morphologically different in adult, but they have still the same major features. Each of the zones receives information from distinct regions of the inferior olive through climbing fibers (CFs) and projects Purkinje cell axons to a certain areas of cerebellar or vestibular nuclei (Ito, 2006). Mossy fibers (MFs) conduct sensory information to cerebellum from the periphery and from cerebral cortex.

The cerebellum is a key component of the motor system. It receives somatosensory input from the spinal cord, motor information from the cerebral cortex, and input from the vestibular organs in the inner ear. The signals to and from the cerebellum are associated with the programming and executing of movement. The cerebellum is not required for muscle contraction or sensing, the basic elements of perception or movement, but it has a crucial role in adjusting the movement. Important features like spatial accuracy, temporal coordination, balance, motor learning and certain cognitive

functions are hindered if the cerebellum is removed (Ghez and Thach, 2000). It has also been suggested that the cerebellum has cognitive and emotional functions in addition to motor and autonomic functions (Apps and Garwicz, 2005; Ito, 2006).

2.1.2 Cerebellar cortex

The cerebellar cortex consists of three layers and seven types of neurons (Ito, 2006). An overview of the cerebellar cortex is presented in Figure 2.1. Molecular layer is the outermost. This layer contains inhibitory stellate and basket interneurons, the axons of granule cells, and the dendrites of Purkinje cells. Inhibitory neurons suppress the activity of the contiguous neurons. The axons of granule cells run parallel to the long axes of the convolutions of cerebellum (*folia*) and are therefore called parallel fibers (PF). PFs pass the dendritic trees of Purkinje cells and form synaptic contacts with Purkinje cells.

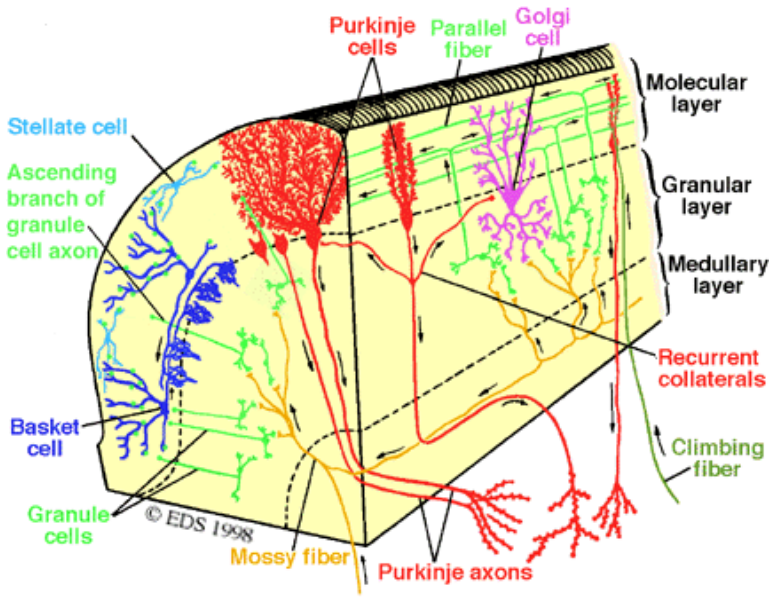

Figure 2.1. *Layers, fibers, and neurons in the cerebellar cortex. The Purkinje cell layer of cerebellar cortex is not mentioned, but it is between the molecular and granular layers. Lugaro interneurons and unipolar brush cells are not drawn. Medullary layer refers here to the beginning of white matter. Adapted from http://www.tnb.ua.ac.be/models/; 11 May 2007 by permission from the author.*

Below the molecular layer is the Purkinje cell layer, which is composed of Purkinje cell bodies, somas. The axons of Purkinje cells go trough the next layer, the granular layer, to the deep cerebellar or vestibular nuclei. Granular layer is the innermost layer of cerebellar cortex. It consists of a very large number of excitatory granule cell, fewer but

larger Golgi and Lugaro interneurons, and in some regions also of unipolar brush cells. Lugaro cells have been long known to exist, but the unique inhibitory function of these cells has been characterized recently (Ito, 2006). Unipolar brush cells are located mainly in the vestibulocerebellum, a part of the cerebellum which receives the primary vestibular afferent nerves (Ito, 2006). The granular layer borders on mossy fibers (MFs), which terminate forming characteristic rosette structures, *glomeruli*, with both excitatory synapses on the dendrites of granule cells and axons of Golgi cells (Ghez and Thach, 2000; Ito, 2006). MFs carry sensory information from the periphery and from cerebral cortex. There is also the third kind of fibers, climbing fibers (CFs), in the cerebellar cortex. CFs begin from the inferior olivary nucleus, which is a part of medulla oblongata. They bring information from different cutaneous receptive fields.

The structure of cerebellar circuitry is well known, but the role of its cells, for example the Lugaro cells, is not yet completely clear. The main pathway of information processing in cerebellum is the three-neuronal pathway, which proceeds from MFs to granule cells and furthermore to Purkinje cells (see Figure 2.2). Other cells in the cerebellum contribute to this pathway by modifying and tuning the signals and affecting on its output (Ito, 2006).

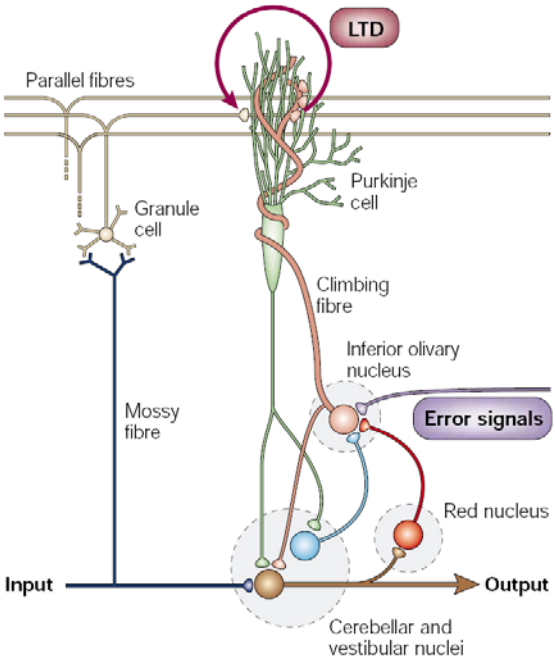

Figure 2.2. *Basic neuronal circuit in cerebellum. LTD (long-term depression). Adapted by permission from Macmillan Publishers Ltd: Nature Reviews Neuroscience* http://www.nature.com/reviews/neuro/ *(Ito, 2002), copyright (2002).*

2.2 Purkinje cell

2.2.1 Structure and functional role

The cerebellar Purkinje cell is one of the largest neurons found in vertebrate brain. Because of its large size, this neuron has been extensively studied with experimental methods. As mentioned in Section 2.1, Purkinje cells are located in the cerebellar cortex. Their extensive dendritic trees spread out to the molecular layer, the somas are located in the Purkinje cell layer, and the axons run through the granular layer to the deep cerebellar or vestibular nuclei (see Figure 2.1) (Ghez and Thach, 2000).

Purkinje cell receives excitatory and inhibitory inputs. The main inputs are excitatory and they are received from the parallel fibers (the axons of granule cells, PFs) and the climbing fibers (CFs). One Purkinje cell receives typically input from several thousands PFs and one CF. An action potential from CF generates an extend voltage-gated Ca^{2+} conductance in the soma and dendrites of Purkinje cell that then lead to prolonged depolarization. This in turn produces a complex spike which is an initial large-amplitude spike followed by a high-frequency burst of smaller-amplitude action potentials (Ghez and Thach, 2000). On the contrary, PFs generate a single action potential or simple spike. Purkinje cell needs simultaneous input from both CF and PFs to fire (Ghez and Thach, 2000).

It has been suggested that 50 simultaneously active granule cells are enough to excite a single Purkinje cell (Barbour, 1993). Stellate and basket cells provide the inhibitory input to Purkinje cell. The stellate cells form neurotransmitter γ-aminobutyric acid (GABA) -mediated synapses to Purkinje cells dendrites whereas the basket cells supply synapses to the bottleneck of a Purkinje cell soma (pinceau). One Purkinje cell can receive input from 20 to 30 basket cells. The stellate and basket cells also have synaptic contact with PFs and therefore these cells mediate the feedforward inhibition of Purkinje cells contribution to PF-Purkinje cell pathway. The output of Purkinje cell is inhibitory and mediated by GABA. As being the output of cerebellar cortex, Purkinje cell has an important role in the overall function of cerebellum (Ito, 2006).

2.2.2 Dendritic spines

Purkinje cell dendrites have a high spine density. Dendritic spines are small bud-like protrusions from the main shaft of dendrite (see Figure 2.2) and they can be found in various types of neurons. Spines consist of a head (volume ~0.01-1 μm^3) and a thin neck (diameter ~0.1 μm), which is attached to a dendrite (see Figure 2.3) (Harris, 1999; Sabatini et al., 2001). The neck functions as a diffusion barrier between the spine and dendrite but the neck is perhaps not restrictive enough to impede synaptic current from proceeding (Sabatini et al., 2001). It has been suggested that by liming the spread of calcium the neck provides input specificity for the synapses and protects the dendritic shaft and soma from the degenerative consequences of calcium-induced toxicity like breakdown of microtubules and dendritic swelling (Harris, 1999). In contrast to Ca^{2+} which is rapidly associated with buffers, IP_3 is able to diffuse through the neck between the spine and dendritic shaft (Augustine et al., 2003). The majority of the synapses in Purkinje cell dendrites are formed at the heads of the spines. Most of the dendritic spines in Purkinje cells include intricate smooth endoplasmic reticulum (SER, marked as ER in the following text) and that is an extension of the ER in dendrite (Sabatini et al., 2001). Every spine head contains a postsynaptic density (PSD) that occupies ~10% of the spine surface. It is a membrane-associated organelle, which contains receptors, channels, signaling molecules and cytoskeletal proteins (see Figure 2.3).

The overall physiological significance of spines in brain is not yet clear, and it is under debate if spines isolate and integrate synaptic signals by compartmentalizing messengers like Ca^{2+} (Schmidt et al., 2007). In addition to the various different volumes, spines also vary a lot in shape and molecular structure (Harris, 1999; Hering and Sheng, 2001). It has been suspected that structural differences in spines can have important functional role in Purkinje cells and also in other neurons (Harris, 1999; Hering and Sheng, 2001; Kennedy et al., 2005; Lee et al., 2005; Santamaria et al., 2006).

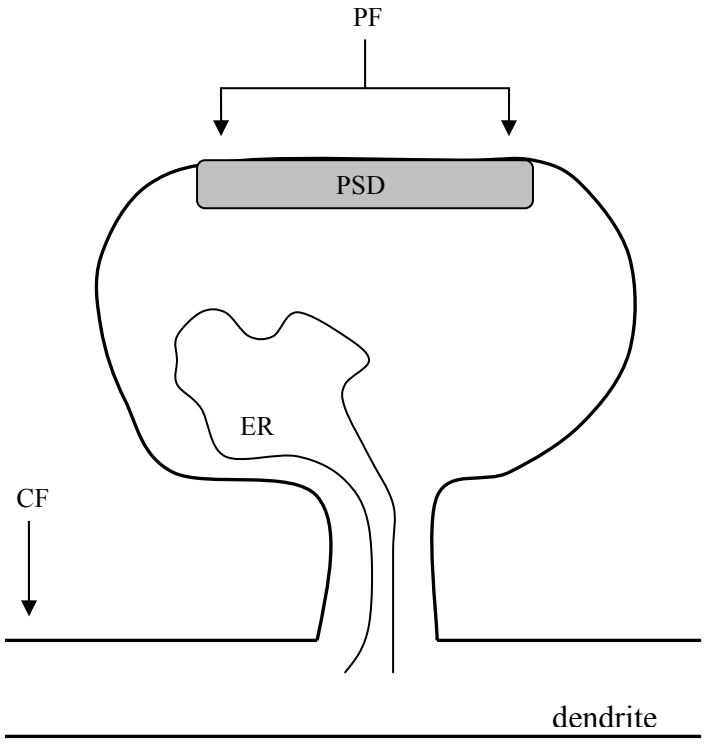

Figure 2.3. *Schematic figure of dendritic spine in Purkinje cell. PF (parallel fiber input), CF (climbing fiber input), PSD (post-synaptic density), ER (endoplasmic reticulum).*

2.2.3 Role of calcium

Calcium ion (Ca^{2+}) is a ubiquitous intracellular messenger. It can be used in signaling because its concentration in cytosol is typically kept low, ~0.1 μM, which is many orders of magnitude below the extracellular Ca^{2+} concentration (~ 1mM) (Alberts et al., 2002). In general, Ca^{2+} is involved in a great amount of different cellular events such as fertilization, muscle contraction, neurotransmitter release, vesicle secretion, gene transcription, immunity and apoptosis (Alberts et al., 2002; Banerjee and Hasan, 2005; Iino, 2006). In neurons, Ca^{2+} is one of the most important intracellular messengers and it has also a crucial role at least in morphogenesis, synaptic plasticity and neurodegeneration (Rizzuto, 2001). There is hardly any reaction in brain that would not be regulated, directly or indirectly, by Ca^{2+}. For this reason it is important to have selective triggering of different controlling systems. This can be accomplished by spatial localization of the Ca^{2+} signals (Augustine et al., 2003). Dendritic spines in Purkinje cells are a good example of separated cell section where localized Ca^{2+} signaling occurs. In general, Ca^{2+} is involved in similar processes in Purkinje cell than in other neurons.

Synaptic plasticity includes long-lasting and activity-dependent changes in synaptic strength. These properties are regarded as the key elements to explain the cellular and molecular mechanisms behind the formation of memory and learning. Synaptic plasticity is triggered in dendrites by a signal transduction cascade which involves always elevation of cytosolic Ca^{2+} concentration. This cascade can induce LTP (long-term potentiation of synaptic strength) or LTD (long-term depression of synaptic strength). The signal transduction cascade behind LTD is described and the essential role of Ca^{2+} is clarified in the Section 2.3.

There are several different Ca^{2+} channels on cell membrane through which Ca^{2+} enters the cell. Among the most significant channels are the voltage-gated Ca^{2+} channels (VGCCs) that response to the changes in membrane potential. There are several different types of VGCCs which are activated in different voltage levels and whose inactivation rates vary from type to type. Some neurotransmitter receptors operate as Ca^{2+} channels. For example, NMDA (N-methyl-D-asparate) receptor (NMDAR) is an ionotropic glutamate receptor that allows the entry of Ca^{2+} in addition to sodium (Na^{+}) and potassium (K^{+}). However, the NMDARs are not expressed in Purkinje cells (Sabatini et al., 2001). AMPA (α-amino-3-hydroxy-5-methylisoxazole-4-propionic acid, an artificial analog of glutamate) receptor (AMPAR) is also an ionotropic glutamate receptor, which releases Na^{+} from extracellular space to cytosol. AMPARs affect cytosolic Ca^{2+} concentration indirectly, because Na^{+} influx produces excitatory post-synaptic current (EPSC) that can open the VGCCs.

Ca^{2+} can be also stored in and released from intracellular stores such as ER, Ca^{2+} buffers or, mitochondria. There are two types of Ca^{2+} channels located on ER: inositol-1,4,5-trisphosphate (IP_3) receptors (IP_3R) and ryanodine receptor (RyR). Purkinje cell spines have lots of IP_3Rs but they totally lack RyRs. However, RyRs are expressed in the dendritic shaft. Ca^{2+} is highly buffered in spines by Ca^{2+} binding protein such as calmodulin, parvalbumin or calbindin (Augustine et al., 2003). The Ca^{2+} concentration in cytosol is kept low by pumping the excess Ca^{2+} to the stores or out of the cell. Into ER, Ca^{2+} is extruded by SERCA (sarcoplasmic/endoplasmic reticulum calcium ATPase) and out of the cell by PMCA (plasma membrane Ca^{2+}-ATPase). In neurons, Ca^{2+} can be also transported out with Na^{+}-driven Ca^{2+} exchanger which joins the efflux of Ca^{2+} to

influx of Na^+. The components that affect directly Ca^{2+} concentration in Purkinje cell spines are illustrated in Figure 2.4.

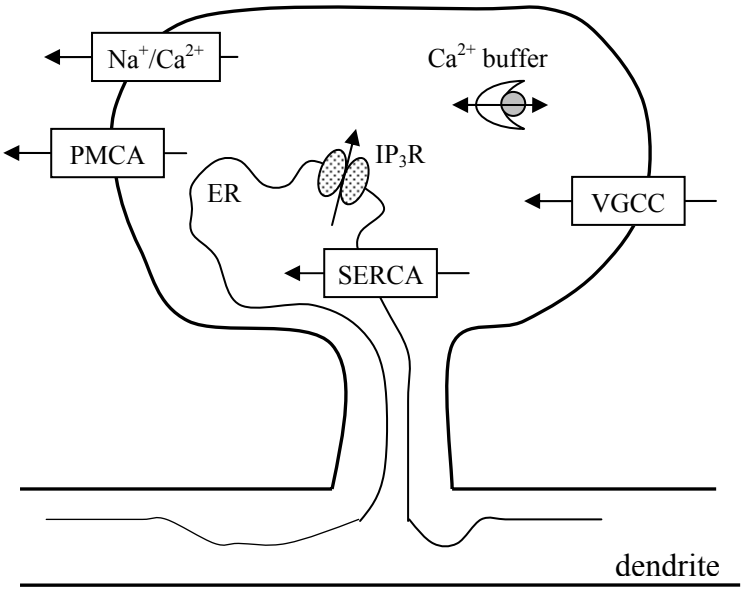

Figure 2.4. *Components affecting directly calcium concentration in Purkinje cell dendritic spine. Arrows indicate the direction of Ca^{2+} flux. Na^+/Ca^{2+} (Na^+-driven Ca^{2+} exchanger), PMCA (plasma membrane Ca^{2+}-ATPase), IP_3R (inositol-1,4,5-trisphosphate receptor), VGCC (voltage-gated Ca^{2+} channel), SERCA (sarcoplasmic/endoplasmic reticulum calcium ATPase), ER (endoplasmic reticulum).*

2.3 Long-term depression

2.3.1 General aspects

Long-term depression (LTD) of synaptic strength is a unique and characteristic form of synaptic plasticity. During LTD the excitability of a neuron is lowered. LTD has been first observed in cerebellar Purkinje cells in early 1980s with new electrophysiological method by recording the firing probabilities of Purkinje cells (Ito et al., 1982; Ekerot and Kano, 1985; Ito, 2006). Later different types of LTD have been found to exist in hippocampus and cerebral neocortex (Ito, 2001). Nowadays, it is strongly believed that LTD has an important role in cerebellar motor learning (Ghez and Thach, 2000; Ito, 2006).

In Purkinje cells, LTD is induced by the simultaneous stimuli from parallel fibers (PFs) and climbing fiber (CF) (Ghez and Thach, 2000; Ito, 2001; Ito, 2006). It has been experimentally shown that a strong PF stimulus alone can induce LTD, but this kind of LTD does not have an influence on learning (Doi et al., 2005). The effect of PF and CF stimulus is supralinear (Wang et al., 2000; Doi et al., 2005), which means that the overall effect of the simultaneous stimuli is grater than the sum of each stimulus alone. The changes in cytosolic Ca^{2+} concentration following PF and CF inputs have been shown to be supralinear in Purkinje cells (Wang et al., 2000). The Ca^{2+} signals are found to have an important role in LTD induction (Ito, 2001; Augustine et al., 2003).

On the molecular level, LTD is basically due to the phosphorylation and removal of AMPARs from subsynaptic plasma membrane. However, before AMPARs can be removed a large amount of biochemical reactions need to occur. There have been three different strategies when trying to create a functionally reasonable organization of all the molecules identified to be involved in LTD induction: 1) identification of mediator and modulator molecules, 2) identification of the coincidence detector mechanism, and 3) analysis the signal transduction pathways (Ito, 2002). All these strategies are well reviewed by Ito (2002). A molecule or ion that is essential for LTD induction is called mediator. A modulator regulates the mediators and their functions. Coincidence detector mechanism detects the simultaneous PF and CF inputs.

2.3.2 Signal transduction

The signal transduction processes behind LTD induction and more particularly behind the two stimulating inputs, PF and CF, in Purkinje cells are quite well known. They are represented in Figure 2.5. By releasing glutamate (Glu) PFs activate δ2 receptor (δ2R) and both PF and CF activate type 1 metabotropic glutamate receptor (mGluR1) and AMPARs. The signal transduction following the activation of δ2R is not yet completely understood, but it is known to associate with tyrosine phosphatase (Ito, 2002). AMPARs cause indirectly elevation in the cytosolic Ca^{2+} concentration as described in previous section (2.2.3) and are also somehow associated with a certain type of protein tyrosine kinase (PTK). mGluR1, in turn, activates phospholipase C (PLC) and most likely phospholipase A_2 (PLA_2) through different G proteins. PLC hydrolyses phosphatidylinositol 4,5-bisphosphate (PIP_2) to diacylglycerol (DAG) and IP_3. DAG

activates protein kinase C (PKC) and IP_3 triggers the release of Ca^{2+} via IP_3R. PLA_2 produces arachidonic acid (AA) and oleic acid from membrane phospholipids. AA also activates PKC (Alberts et al., 2002; Ito, 2002).

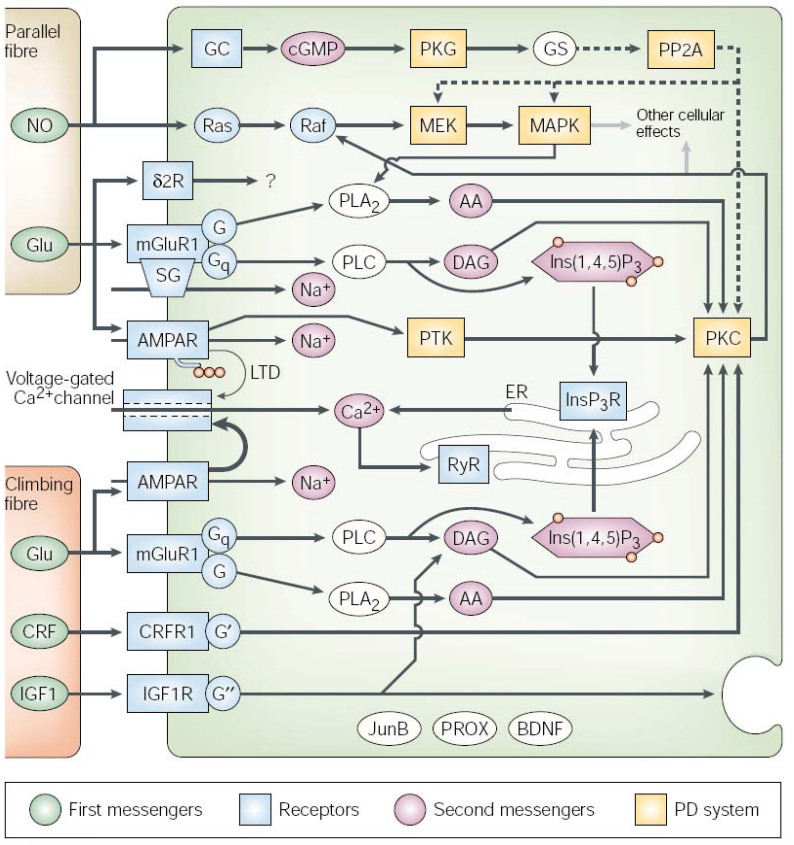

Figure 2.5. *Signal transduction network after stimulation of PF (parallel fiber) and CF (climbing fiber). Solid lines signify activation and dash line signify inactivation. JunB (immediate-early gene product that is expressed during long-term depression (LTD)), PROX (protein that has role in LTD induction), δ2R (δ2receptor), AA (arachidonic acid), AMPAR (α-amino-3-hydroxy-5-methylisoxazole-4-propionic acid receptor), BNDF (brain-derived neurotrophic factor), CRF (corticotrophin-releasing factor), CRFR1 (CRF type 1 receptor), DAG (diacylglycerol), ER (endoplasmic reticulum), GC (guanylyl cyclase), Glu (glutamate), GS (G-substrate), IGF1 (insulin-like growth factor 1), IGF1R (IGF1 receptor), $Ins(1,4,5)P_3$ (IP_3, inositol-1,4,5-trisphosphate), $Ins(1,4,5)P_3R$ (IP_3R, $Ins(1,4,5)P_3$ receptor), MAPK (mitogen-activated protein kinase), MEK (MAPK kinase), mGluR1 (type 1 metabotropic glutamate receptor), NO (nitric oxide), PD (phosphorylation-dephosphorylation), PKC (protein kinase C), PKG (protein kinase G), PLA_2 (phospholipase A_2), PLC (phospholipase C), PP2A (protein phosphatase 2A), PTK (protein tyrosine kinase), RyR (ryanodine receptor), SG (slow-EPSP generator associated with mGluR). Adapted by permission from Macmillan Publishers Ltd: Nature Reviews Neuroscience http://www.nature.com/reviews/neuro/ (Ito, 2002), copyright (2002).*

In addition to Glu, PFs release also another neurotransmitter, nitric oxide (NO). NO diffuses freely through membranes, because it is a gas. In post-synaptic area, it activates

guanylyl cyclase (GC) and possibly RAS-RAF-pathway, which eventually activates mitogen-activated protein kinase (MAPK) via MAPK kinase (MEK). The activation GC results in the production of cyclic GMP (cGMP) which then activates protein kinase G (PKG). In Purkinje cells PKG has a specific protein substrate, G-substrate. PKG phosphorylates G-substrate, which can then inhibit protein phosphatases like protein phosphatase 2A (PP2A) (Ito, 2002).

CFs also release two types of peptides, CRF (corticotropin-releasing factor) and IGF1 (insulin-like growth factor 1), in addition to Glu. CRF binds to type 1 CRF receptor (CRFR1) and activates it. This leads to the translocation of PKC to plasma membrane. IGF1 activates IGFR1 receptor (IGF1R), which then induces the production of DAG. Thus, both CRF and IGF1 contribute to the activation of PKC. It is also thought that IGF1 is involved in LTD induction by promoting endocytosis (Ito, 2002).

It has been suggested that the primary mediator of LTD induction could be the mGluR1-IP_3R-Ca^{2+} release pathway and secondary mediator could be the AMPAR-VGCC-Ca^{2+}-entry pathway (Ito, 2002). Ito (2002) has also named four candidates to be the coincidence detectors: IP_3Rs, VGCCs in spines, phosphorylation-de phosphorylation system, and AMPARs related to PF stimulus.

2.4 IP_3 receptor

2.4.1 Structure and function

Inositol-1,4,5-trisphosphate (IP_3) receptor (IP_3R) is a membrane-bound protein containing a Ca^{2+} channel regulated by Ca^{2+} and IP_3. IP_3Rs are mainly expressed on ER and their function is to release Ca^{2+} from ER to cytosol. IP_3Rs have also been found to mediate the Ca^{2+} release from other organelles like nuclear envelope, Golgi apparatus, and secretory vesicles. IP_3Rs are also located in the plasma membrane in some cell types (Taylor et al., 2004). It has been observed that IP_3Rs are spatially organized in high density clusters (Banerjee and Hasan, 2005).

IP_3R is a large protein (>1 MDa) and there are at least three types of IP_3R found in mammals: IP_3R1, IP_3R2, IP_3R3 (Maeda et al., 1989; Yamamoto-Hino et al., 1994; Taylor et al., 2004). All the three types consist of four subunits (Taylor et al., 2004). Based on the sequence analysis, it has been suggested that each subunit has a single IP_3 binding site, but the exact location of the binding sites is still contentious (Taylor et al., 2004). Each type has different steady-state and kinetic properties and they are also expressed in different proportions in different cell types (Sneyd and Falcke, 2005). The type 1 IP_3R (IP_3R1) is the most common and it is also the main type found in neurons (Banerjee and Hasan, 2005). There are exceptionally high levels of IP_3R1 in Purkinje cells and their spines (Maeda et al., 1989; Sharp et al., 1999). In general, all types of IP_3R have the same function and they are regulated by the same factors, IP_3 and Ca^{2+}. Also some additional mediators have been found to exist: ATP (Patel et al., 1999) and calmodulin (Taylor et al., 2004).

The three dimensional structure of IP_3R1 has been studied by electron microscopy (EM). More traditional techniques, such as NMR (nuclear magnetic resonance) or X-ray crystallography, cannot be used effectively because IP_3R is a large protein bound to membrane. Based on EM images, IP_3R1 purified from mouse cerebellum has two Ca^{2+}-dependent 3D conformations: a windmill structure and a square structure (Hamada et al., 2002; Hamada et al., 2003). The two conformations are represented in Figure 2.6. When Ca^{2+} is present IP_3R takes the windmill structure, presumable an active state. This supports the assumption that Ca^{2+} acts as a regulator for IP_3-triggred IP_3R1 activation. Hamada et al. (2003) has also proposed that the square structure, presumable a resting state of the IP_3R1, has mushroom-like side view consisting of a square-shaped head and a smaller channel domain with bridges (Hamada et al., 2003). Based on the studies of both 3D conformations, Hamada et al. (2003) has suggested that the conformational changes from square to windmill are due to the relocation of functional domains.

It is thought that several or all of the subunits of IP_3R need to bind IP_3 to achieve stable open state (Marchant and Taylor, 1997; Taylor et al., 2004), but some data about spontaneous opening without IP_3 in very low Ca^{2+} concentration has also been published (Mak et al., 2003). The details of the co-operation of the two regulators are not yet fully understood, but it is known that binding of IP_3 has two important consequences: it inhibits the binding of Ca^{2+} to an inhibitory site and permits Ca^{2+} to bind to stimulatory

site (sequential binding) (Taylor et al., 2004). The latter promotes the opening of an ion channel. Because IP_3R is regulated by Ca^{2+}, it can respond to its own activity and affect also the activities of nearby IP_3Rs (Taylor et al., 2004). This causes Ca^{2+} sparks, which are sudden localized increases in cytosolic Ca^{2+} concentration (or puffs). Ca^{2+} puffs have been detected in experiments with *Xenopus laevis* oocytes (see for example Yao et al., 1995). An important feature of IP_3R is that it is one of the factors in cell responsible for a phenomenon, Ca^{2+}-induced Ca^{2+} release (CICR), where release of a small amount of Ca^{2+} causes a larger release (Rizzuto, 2001). Another thing promoting the sparks is the short distance between clustered IP_3Rs. Sparks have been found in many types of cells including some neurons (Melamed-Book et al., 1999).

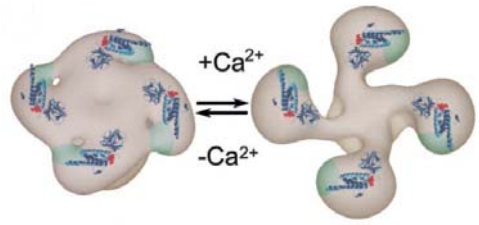

Figure 2.6. *Illustration of two Ca^{2+}-dependent conformations of IP_3R. On the left, there is a square-like conformation and on the right a wind-mill conformation. Adapted by permission from ASBMB Journals: (Hamada et al., 2003).*

Experimental studies of cerebellar IP_3R have shown that the open probability of IP_3R at steady-state has a bell-shaped curve for dependence on cytosolic Ca^{2+} concentration (Bezprozvanny et al., 1991). In their studies (Bezprozvanny et al., 1991), the IP_3R was first isolated in vesicles from canine cerebellum and then fused to planar lipid layer. It is shown that the open probability of IP_3R increased when cytosolic Ca^{2+} concentration raised from 0.1 μM to 0.25 μM and decreased above 0.25 μM. Similar results have been obtained later (Kaznacheyeva et al., 1998), and also with other cell types (Iino, 1990; Parys et al., 1992). When IP_3 and Ca^{2+} concentrations are altered the curve changes it shape (Bootman and Lipp, 1999). For example, when IP_3 concentration is high and the inactivation of IP_3R by Ca^{2+} is inhibited, the curve moves to the right and the steepness of the curve reduces from the right side of the curve (Bootman and Lipp, 1999). The bell-shaped dependence of cytosolic Ca^{2+} concentration can only be obtained if Ca^{2+} both activates and inactivates IP_3R in different concentrations.

2.4.2 Models of IP_3 receptor

Several mathematical models have been proposed for IP_3R function (for a review, see Sneyd and Falcke, 2005). Some of the most popular and recent ones including steady-state, dynamic, allosteric, and stochastic models are introduced in this Section. Many qualitative or conceptual models have been also proposed and they have been very important in understanding the properties and behavior of IP_3R. Additionally, they have greatly helped in developing new mathematical models of IP_3R (Sneyd and Falcke, 2005). Different types of IP_3R behave differently in contrast to other. The environment of the receptor also influences the behavior crucially. This means that each of the models published so far is actually tuned to show a correct behavior but in many cases only in one situation.

Early IP_3R models, like De Young-Keizer model (De Young and Keizer, 1992), have been developed to reproduce the cytosolic oscillations of Ca^{2+} concentration and the bell-shaped curve of open probability at steady-state, but not dynamic properties like the responses to changes in cytosolic Ca^{2+} and IP_3 concentrations. These models also take into account the conclusion based on experimental findings that Ca^{2+} activates the IP_3R fast and inactivates it slowly (Sneyd and Falcke, 2005). De Young-Keizer model is one of the oldest and most used models among all IP_3R models. In this model, it is assumed that the IP_3R has three equivalent and independent subunits. Each subunit has one IP_3 binding site and two Ca^{2+} binding sites, one for activating and another for inhibiting, and therefore, eight different states. IP_3R is considered as open when all the subunits are in a same certain state. The parameters or rate constants of De Young-Keizer model have been chosen so that the model reproduces the experimental data of Bezprozvanny et al. (Bezprozvanny et al., 1991). As the structure and function of IP_3R has clarified, some parts of De Young-Keizer model are not valid anymore. Firstly, IP_3R has four subunits instead of three as discussed in the Section 2.4.1. Secondly, experiments have shown that the binding of IP_3 and Ca^{2+} is likely sequential and not independent (Taylor et al., 2004). It is also thought that, when activating, IP_3R binds first IP_3 and then Ca^{2+}. Li and Rinzel (1994) have published a mathematical simplification of the De Young-Keizer model. This model has been used for example in a study analyzing stochastic properties of Ca^{2+} release from IP_3R clusters (Shuai and Jung, 2002). Atri et al. (1993) have introduced a model which has structural similarities with De Young-Keizer model

and an inactivation variable. In addition to these binding models, Othmer and Tang (1993) and Bezprozvanny (1994) have introduced structurally similar models with sequential binding.

There has been published an extended version of De Young-Keizer model including, for example, four subunits instead of three. This extended model (Kaftan et al., 1997) has been later improved by the same group (Moraru et al., 1999). The model has been constructed to reproduce the steady-state data from canine cerebellum and type 1 IP_3R as well as the open times of the IP_3R as a function of cytosolic Ca^{2+} concentration. In this model, IP_3R has 125 states (Sneyd and Falcke, 2005). Mak and Foskett (2001) have introduced a phenomenological steady-state model based on their experimental data on types 1 and 3 IP_3R in *Xenopus laevis* oocytes. In this model, there is an equation for open probability of the receptor and states of IP_3R are not particularly defined. All these models produce steady-state features of the IP_3R satisfactorily.

The problem with steady-state models is that rarely a steady Ca^{2+} concentration can be observed in cells. Thus, from the biological point of view the response to changing Ca^{2+} concentration is at least as important as the steady-state response. LeBeau et al. (1999) have published dynamic model of type 3 IP_3R in pancreatic acinar cells. The structure of the model is somewhat different from other models thus far. The main distinctive feature in this model is that IP_3R does not bind Ca^{2+}. Instead, Ca^{2+} modulates the affinity of IP_3 binding. Although the model is not completely correct, it predicts that different agonists lead to different phosphorylated states of IP_3R (this has been later confirmed with experiments) and it shows that Ca^{2+} oscillation can be created even though the open probability curve is not bell-shaped (Sneyd and Falcke, 2005). Sneyd and Dufour (2002) have presented an improved version of the IP_3R model of LeBeau et al. (1999). The model includes several features suggested by experiments including for example sequential binding of IP_3 and activating Ca^{2+} and fitting to dynamic data instead of steady-state data only (Sneyd and Falcke, 2005). In the model, IP_3R has six states and the rates of its reactions are not based on the law of mass action (which is discussed in the Section 2.5) but on specific functions. Parameter values of the model have been determined by using time series data from experiments on type 2 IP_3R (Sneyd and Falcke, 2005). Doi et al. (2005) have introduced a kinetic model of IP_3R based on a conceptual model of Adkins and Taylor (1999). In this model, IP_3R requires sequential

binding of IP_3 and Ca^{2+}. The model has been published as a part of a larger model for Ca^{2+} release in Purkinje cell spine and it is presented in more detail in the Section 4.1.1.

Some allosteric models have also been proposed for IP_3R by Laurent and Claret (1997), Dawson et al. (2003), and Mak et al. (2003). In allosteric models, it is assumed that IP_3R has two conformations which both have different affinities for IP_3 and Ca^{2+} binding. The model of Laurent and Claret (1997) has been constructed based on steady-state data by Bezprozvanny et al. (1991). Dawson et al. (2003) have introduced a model that is applicable for types 1 and 2 IP_3R and with some modifications also to type 3. This model can provide a possible explanation how Ca^{2+} flux can stop although positive feed-back from released Ca^{2+} is available (Dawson et al., 2003). After the phenomenological model at 2001, Mak et al. published in 2003 a somewhat complex allosteric model with 3750 states. It is based on the very same data as the previous model, but it also incorporates new data from *Xenopus laevis* oocytes.

The last group of IP_3R models introduced here are the stochastic models. Swillens et al. (1998) have published a model with two features of IP_3R: bell-shaped curve for open probability and decreased mean open time as Ca^{2+} flux is increased. They use random numbers to create the stochastic behavior for single IP_3R. This model also includes diffusion that is not modeled as stochastic. They are able to simulate the burst-like activity of IP_3R with repetitive channel openings. Fraiman and Dawson (2004) are the first ones to introduce a model of IP_3R with a luminal Ca^{2+} site. Thereby the amount of Ca^{2+} in the ER also affects the behavior of the receptor. The model of Fraiman and Dawson (2004) is discussed in more detail in Section 4.1.2.

Falcke (Falcke, 2003) have presented a stochastic model for intracellular Ca^{2+} oscillations. The model includes deterministic diffusion and a stochastic channel dynamics of IP_3R for which De Young-Keizer model is used as a basis. The model is able to produce both long and short period oscillations with a model containing cluster of IP_3Rs. The deterministic version of the model can not produce the oscillations. Diambra and Guisoni (2005) and Shui and Jung (2002) have also modeled a cluster of IP_3Rs. They present a stochastic procedure to simulate different IP_3R models. Diambra and Guisoni use the model of Othmer and Tang (1993) and Shui and Jung (2002) use the model of Li and Rinzel (1994). The results from the study of Diambra and Guisoni

(2005) suggest that the feedback from cytosolic Ca^{2+} has an important role in the response of IP_3R to IP_3. Shui and Jung (2002) show the similar release of Ca^{2+} than observed experimentally. Means et al. (2006) have introduced a reaction diffusion model of the Ca^{2+} dynamics in mast cell with realistic ER geometry including also a model for IP_3R. They use a structurally similar model presented by Bezprozvanny and Ehrlich (1994) with parameter values based on experimental data by Tu et al. (2005a; 2005b). Haeri et al. (2007) have simulated a single subunit of De Young-Keizer model using Gillespie algorithm (see Section 2.6.2). They conclude that Gillespie algorithm is a good choice for studying such systems.

None of the models introduced here is perfect or the final model of IP_3R. These models have good properties and they have efficiently promoted the development of the ultimate IP_3R model.

2.5 Modeling with ordinary differential equations

2.5.1 Formulation of ordinary differential equation system

A series of biochemical reactions constitutes a biochemical system such as a signal transduction network or a metabolic pathway. The time series behavior of a biochemical system can be mathematically described, i.e. modeled, using ordinary differential equations (ODEs) and the law of mass action (described in Zumdahl, 1998). A model can have inputs, whose concentrations do not change with the model but are determined by a constant value or by an equation, for example a sine wave. The formulation of ODEs in this section is based on several sources: (Copeland, 2000; Leckovac, 2003; Turner et al., 2004; Manninen et al., 2006b; Kinetikit manual, 2006).

Each reaction in a biochemical system can be described using the law of mass action (described in Zumdahl, 1998). An example of simple reaction can be given as

$$\mathrm{A} \xrightarrow{k_f} \mathrm{B} + \mathrm{C} \tag{2.1}$$

where A is the reactant and C and B are the products. k_f is the forward rate constant. The rate of the reaction (below marked as v) in Equation 2.1 can be described by

$$v = v_f = k_f[\mathrm{A}], \tag{2.2}$$

where [A] is the concentration of species A. The consumption rate of species A and the formation rates of B and C can be described using ODEs

$$\frac{\mathrm{d[A]}}{\mathrm{d}t} = -v \tag{2.3}$$

$$\frac{\mathrm{d[B]}}{\mathrm{d}t} = \frac{\mathrm{d[C]}}{\mathrm{d}t} = v, \tag{2.4}$$

where v is as given in Equation 2.2, and [B] and [C] are the concentrations of species B and C. If the reaction is reversible, the rate of backward reaction also influences the reaction rate v. The rate of backward reaction for reaction given in Equation 2.1 is

$$v_b = k_b[\mathrm{B}][\mathrm{C}], \tag{2.5}$$

where v_b is the reaction rate, k_b is the backward rate constant. The total rate of the reversible reaction is therefore

$$v = v_f - v_b = k_f[\mathrm{A}] - k_b[\mathrm{B}][\mathrm{C}]. \tag{2.6}$$

The ODEs for each species in a reversible reaction are as in Equations 2.3 and 2.4 and v is as given in Equation 2.6.

Stoichiometry must also be taken into account in modeling. For example, if the reaction is the following

$$3\mathrm{A} + \mathrm{B} \underset{k_b}{\overset{k_f}{\rightleftharpoons}} 2\mathrm{C} \tag{2.6}$$

the rate of the reaction becomes

$$v = k_f[\mathrm{A}]^3[\mathrm{B}] - k_b[\mathrm{C}]^2 \tag{2.7}$$

and the ODEs for each species are

$$\frac{\mathrm{d[A]}}{\mathrm{d}t} = -3v \tag{2.8}$$

$$\frac{\mathrm{d[B]}}{\mathrm{d}t} = -v \tag{2.9}$$

$$\frac{\mathrm{d[C]}}{\mathrm{d}t} = 2v. \tag{2.10}$$

Generally, for a reaction

$$a\mathrm{A} + b\mathrm{B} \underset{k_b}{\overset{k_f}{\rightleftharpoons}} c\mathrm{C} + d\mathrm{D} \tag{2.11}$$

the rate of reaction is represented as follows

$$v = k_f[\mathrm{A}]^a[\mathrm{B}]^b - k_b[\mathrm{C}]^c[\mathrm{D}]^d = -\frac{1}{a}\frac{\mathrm{d}[\mathrm{A}]}{\mathrm{d}t} = -\frac{1}{b}\frac{\mathrm{d}[\mathrm{B}]}{\mathrm{d}t} = \frac{1}{c}\frac{\mathrm{d}[\mathrm{C}]}{\mathrm{d}t} = \frac{1}{d}\frac{\mathrm{d}[\mathrm{D}]}{\mathrm{d}t} \quad (2.12)$$

A model that is based on the law of mass action and described using ordinary differential equations can also be represented as

$$\mathrm{d}\mathbf{x}(t) = \mathbf{S}\mathbf{v}(\mathbf{K}, \mathbf{x}(t))\mathrm{d}t \quad (2.13)$$

(Manninen et al., 2006b). In Equation 2.13, **x** is a vector containing the *m* variables (concentrations of species) of the model. **S** is a stoichiometric matrix with dimensions $m \times n$ (*n* is the number of reactions) containing the coefficients of the chemical species. **K** is a matrix containing the rate constants. The function **v** describes the rates of the reactions, which depend on the rate constants **K** and variables **x**. The number of ODEs in a system is always the number of chemical species involved.

2.5.2 Solving ordinary differential equation system

Most of the ordinary differential equation systems cannot be solved analytically and therefore the only way to solve them is to approximate. The approximation can be done by numerical integration i.e. simulation. In practice, during the simulation the concentration of a species (molecule or ion) is calculated as a function of time. In order to be able to run simulations, the initial value (here concentration or quantity) for each reacting species must be set.

Several different integration methods can be used to solve the kind of ODE models described above. A classical and very simple integration method is called Euler's method (described in Eldén et al., 2004), but is rarely used in advanced applications. There are more efficient and accurate methods available, for example Runge-Kutta (described in Eldén et al., 2004) and Exponential Euler methods (described in Bower and Beeman, 1998). In this work, GENESIS/Kinetikit simulation environment (Bower and Beeman, 1998; Bhalla and Iyengar, 1999; Bhalla, 2002) is used for deterministic simulations. It uses the Exponential Euler method as a default solving method (see p. 324 in Bower and Beeman, 1998).

When using the law of mass action based ODEs, it is assumed that the system is well-mixed (every molecule has the same probability to react), continuous, and macroscopic. ODE models are always deterministic. This means that the model produces the same result every time a simulation is run if the simulation settings are not changed. A deterministic model is always a simplification and an approximation of the average behavior of a real system.

2.6 Stochasticity in biological systems

2.6.1 General aspects

Traditionally, deterministic law of mass action based modeling (as in Section 2.5) is used for describing the kinetics of biochemical reactions. However, it is known that biochemical systems have characteristics that are not taken into account in this deterministic approach. Chemical reactions include discrete and random collisions between separate molecules and the molecules are not evenly distributed in a cell. Deterministic models assume that the system is well-mixed, which does not always apply to circumstances in a cell or in its organelles. Concentrations of molecules and ions vary within the cell. When even smaller and smaller systems are considered, the law of mass action becomes inadequate. It is not capable of modeling the specific randomness of a system (Turner et al., 2004). Stochastic modeling has been proposed for describing the dynamics of a biochemical system, since there are at least three aspects that are missing from deterministic approaches. These aspects are: (1) discrete nature of the quantity of components and inherently random nature of modeled phenomena, (2) certain accordance with the theories of thermodynamics and stochastic processes, and (3) suitability for describing small systems and instability phenomena (Turner et al., 2004). The stochastic approach is always valid whenever the deterministic approach is valid, but when the deterministic is not, the stochastic is sometimes valid (Gillespie, 1976).

When aiming at modeling systems inside a single cell or inside a specific part of it, such as a Purkinje cell spine, the environment cannot any more be considered as macroscopic. The volume and the amounts of molecules and ions are extremely small.

In this kind of situation, both the randomness of molecular encounters and the fluctuations in the transitions between the conformational states of proteins become functionally relevant. Stochastic approach should be used in modeling and simulation to achieve results as realistic as possible.

In recent years, the use of stochastic approaches in modeling and simulation of biochemical systems has increased although the methods for this have existed for couple of decades (see, for example, Swillens et al., 1998; Shuai and Jung, 2002; Falcke, 2003; Bhalla, 2004a; Fraiman and Dawson, 2004a; Bhalla, 2004b; Diambra and Guisoni, 2005; Manninen et al., 2006a; Manninen et al., 2006b). The main reason for the delay in applying stochastic methods in computational cell and molecular biology has been the lack of computation capacity. For example, Falcke (2003) has reported that the simulation of the model of Ca^{2+} oscillations for 100 s took several hundred hours of CPU time. Stochastic simulations take even tens of times more time to simulate than deterministic ones. For statistical reasons, it is also necessary to perform multiple repetitions in order to be able to compare the results with deterministic simulation. The number of required repetitions of stochastic simulations depends on the model (Gillespie, 1977).

2.6.2 Gillespie stochastic simulation algorithm

The chemical master equation (CME, not presented here) is a differential-difference equation describing the stochastic dynamics of chemical reaction system. It is mathematically intractable and in most cases impossible to solve analytically, or even numerically (Gillespie, 1977). Gillespie (1976; 1977) has developed a stochastic simulation algorithm (SSA) for simulation of coupled chemical reactions. The SSA is a computational algorithm for numerically calculating the same process that the CME describes analytically (Gillespie, 1977). SSA is a feasible method for numerical calculation of the stochastic time evolution of a system.

In the SSA, the amounts of molecules are represented with discrete numbers of molecules instead of concentrations, but each molecule is not represented individually. The algorithm handles each collision between two molecules or ions as a separate event that occurs with certain probability (Gillespie, 1977). Thus the reaction constants are not

rate constants but reaction probabilities per time unit. Ordinary differential equation systems, similar to the ones represented in Section 2.5.1, can be simulated with the SSA, but the rate constants must be transformed to the correct unit. These, and the quantities of molecules out of concentration, can be calculated using the volume of the system and Avogadro's number.

Basically, what the SSA does is that it generates two separate random numbers. Based on the random numbers, it then determines which reaction occurs and what the duration of the next time step is. When repeating this, a possible individual behavior (realization) of the modeled system is generated. Simulation need to be repeated many times to get in-depth insight of variability occurring in the behavior of the system.

3 Aims of research

The aim of this work was to study the effects of stochasticity on inositol-1,4,5-trisphosphate receptor (IP_3R) functioning in cerebellar Purkinje cell dendritic spine. Two different mathematical models of IP_3Rs were used in two kinds of simulations, deterministic and stochastic. The hypothesis was that the comparison between deterministic and stochastic simulation results provides new insight into the importance of incorporating stochasticity when simulating intracellular events.

4 Methods

4.1 IP_3 receptor models

Many of the IP_3 receptor (IP_3R) models introduced in the Section 2.4.2 could not be used as test cases in this study. The main reasons for rejecting them were that (1) the data used as a basis of the model was not even partially from cerebellum or it was from other type of the IP_3R than type 1, (2) the implementation of the model would have exceeded the duration of a Master's thesis work, (3) the mathematical formulation was not compatible with the simulation software used in this work, and (4) the models were old. Based on an extensive examination of the existing models, two models were selected as test cases: Doi et al. (2005) and Fraiman and Dawson (2004a).

4.1.1 Model of Doi et al. (2005)

The IP_3R model of Doi et al. (2005) has been originally published as a part of a larger model for Ca^{2+} dynamics in the cerebellar Purkinje cell spine. The parameter values of this model have been determined based on experimental data from Purkinje cells (Doi et al., 2005). The model was originally implemented as deterministic within the GENESIS/Kinetikit simulation environment (Bower and Beeman, 1998; Bhalla and Iyengar, 1999; Bhalla, 2002). A schematic representation of the model is shown in Figure 4.1.

In this model, the IP_3R has seven different states and six reversible transitions between these states (see Figure 4.1). IP_3R has five cytosolic Ca^{2+} binding sites and one IP_3 binding site. All the reactions and their rate constants are listed in Table 4.1. In this model, IP_3R needs to bind both IP_3 and Ca^{2+} to open and thus provide Ca^{2+} flux from endoplasmic reticulum (ER) lumen to cytosol. IP_3R has only one open state, RIC, in this model. Rate constants are determined in such a way that large concentrations of Ca^{2+} in cytosol induce inactivation of IP_3R (Doi et al., 2005).

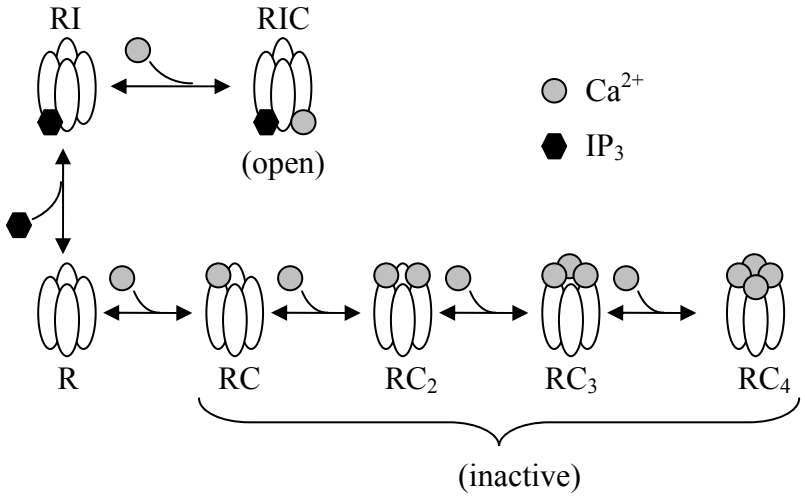

Figure 4.1. *Schematic representation of states and transitions for the IP_3R model of Doi et al. (2005).*

Table 4.1. *Reactions and rate constants for IP_3R model of Doi et al. (2005). k_f is the forward rate constant and k_b is the backward rate constant. The states are consistent with the states in Figure 4.1. 1e9 stands for $1*10^9$ and M=mol/l.*

Reaction	**k_f**	**k_b**
$RI + Ca^{2+} \leftrightarrow RIC$	$8000\frac{1}{\mu Ms} = 8e9\frac{1}{Ms}$	$2000\frac{1}{s}$
$R + IP_3 \leftrightarrow RI$	$1000\frac{1}{\mu Ms} = 1e9\frac{1}{Ms}$	$258000\frac{1}{s}$
$R + Ca^{2+} \leftrightarrow RC$	$8.889\frac{1}{\mu Ms} = 8.889e6\frac{1}{Ms}$	$5\frac{1}{s}$
$RC + Ca^{2+} \leftrightarrow RC_2$	$20\frac{1}{\mu Ms} = 20e6\frac{1}{Ms}$	$10\frac{1}{s}$
$RC_2 + Ca^{2+} \leftrightarrow RC_3$	$40\frac{1}{\mu Ms} = 40e6\frac{1}{Ms}$	$15\frac{1}{s}$
$RC_3 + Ca^{2+} \leftrightarrow RC_4$	$60\frac{1}{\mu Ms} = 60e6\frac{1}{Ms}$	$20\frac{1}{s}$

4.1.2 Model of Fraiman and Dawson (2004)

The IP_3R model of Fraiman and Dawson (2004a; 2004b) has unique characteristics compared to most of the other IP_3R models published. It is the only model having Ca^{2+} binding site inside ER in addition to cytosolic binding sites. Another distinguishing feature is that the conformational changes of the receptor are taken into account. In most

of the other IP_3R models, these changes are presumed to happen indefinitely fast (Fraiman and Dawson, 2004a). A schematic representation of the model is in Figure 4.2.

In this model, IP_3R has 14 states and 14 reversible transitions between the states. Of the 14 transitions, two are IP_3 binding/unbinding reactions, four cytosolic Ca^{2+} binding/unbinding reactions, two ER luminal Ca^{2+} binding/unbinding reactions, and six conformational changes (see Figure 4.2). All the reactions and their rate constants are listed in Table 4.2.

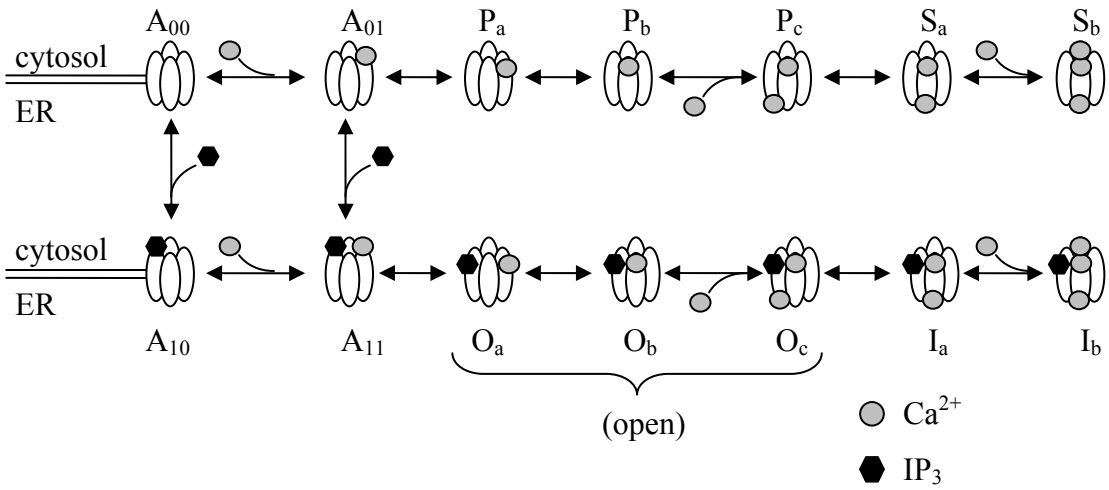

Figure 4.2. *Schematic representation of states and transitions in the IP_3R model of Fraiman and Dawson (2004a).*

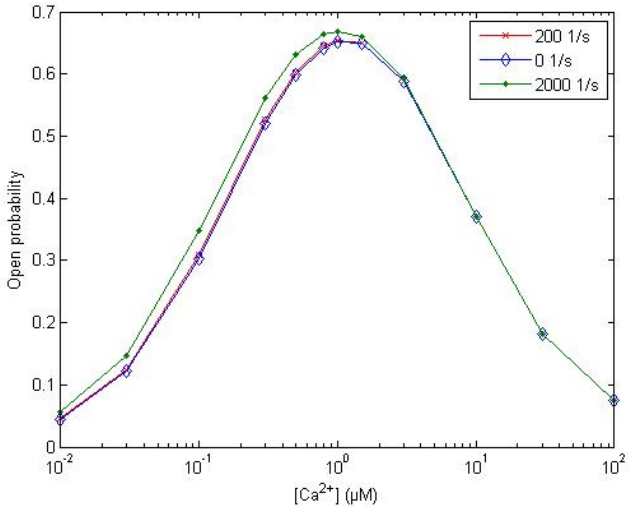

Figure 4.3. *Open probability curves of the model of Fraiman and Dawson (2004a) with three different rate constant values for transition $A_{10} \rightarrow A_{00}$. The value of 200 s^{-1} was selected for the rest of the study.*

Table 4.2. *Reactions and rate constants for IP_3R model of Fraiman and Dawson (2004a, 2004b). k_f is the forward rate constant and k_b is the backward rate constant. The states are consistent with the states in Figure 4.2. 1e9 stands for $1*10^9$ and M=mol/l.*

Reaction	$\mathbf{k_f}$	$\mathbf{k_b}$
$A_{00} + Ca^{2+}_{cyt} \leftrightarrow A_{01}$	$5000\frac{1}{\mu Ms} = 5e9\frac{1}{Ms}$	$1\frac{1}{s}$
$A_{01} \leftrightarrow P_a$	$0.3\frac{1}{s}$	$700\frac{1}{s}$
$P_a \leftrightarrow P_b$	$500\frac{1}{s}$	$100\frac{1}{s}$
$P_b + Ca^{2+}_{ER} \leftrightarrow P_c$	$5000\frac{1}{\mu Ms} = 5e9\frac{1}{Ms}$	$150\frac{1}{s}$
$P_c \leftrightarrow S_a$	$3000\frac{1}{s}$	$250\frac{1}{s}$
$S_a + Ca^{2+}_{cyt} \leftrightarrow S_b$	$5000\frac{1}{\mu Ms} = 5e9\frac{1}{Ms}$	$20\frac{1}{s}$
$A_{00} + IP_3 \leftrightarrow A_{10}$	$6670\frac{1}{\mu Ms} = 6670e6\frac{1}{Ms}$	In this work, this parameter is $200\frac{1}{s}$
$A_{10} + Ca^{2+}_{cyt} \leftrightarrow A_{11}$	$500\frac{1}{\mu Ms} = 500e6\frac{1}{Ms}$	$667\frac{1}{s}$
$A_{01} + IP_3 \leftrightarrow A_{11}$	$1540\frac{1}{\mu Ms} = 1540e6\frac{1}{Ms}$	$18\frac{1}{s}$
$A_{11} \leftrightarrow O_a$	$1800\frac{1}{s}$	$330\frac{1}{s}$
$O_a \leftrightarrow O_b$	$133\frac{1}{s}$	$1500\frac{1}{s}$
$O_b + Ca^{2+}_{ER} \leftrightarrow O_c$	$70\frac{1}{\mu Ms} = 70e6\frac{1}{Ms}$	$2000\frac{1}{s}$
$O_c \leftrightarrow I_a$	$630\frac{1}{s}$	$400\frac{1}{s}$
$I_a + Ca^{2+}_{cyt} \leftrightarrow I_b$	$60\frac{1}{\mu Ms} = 60e6\frac{1}{Ms}$	$16\frac{1}{s}$

In this model also IP_3R needs to bind both IP_3 and Ca^{2+} to open. Originally, in this model the states O_a, O_b, O_c, P_a, P_b, and P_c are considered as open. However, the prevailing believe is that IP_3R needs IP_3 to reach a stable open conformation (Marchant and Taylor, 1997; Taylor et al., 2004). In this work, only states O_a, O_b, and O_c were considered as open to simplify the model and reduce the amount of data to be handled. In the original article by Fraiman and Dawson (2004a, 2004b), the rate constant of the

transition $A_{10} \rightarrow A_{00}$ is defined as 'detailed balance'. Before the model could be used in this work a value for this one parameter had to be determined. Three values were selected and they were tested with deterministic open probability simulation (curves are shown in Figure 4.3). Simulations were done as described in Section 4.3.1. The parameter values of 0 s^{-1} and 200 s^{-1} produced the same results and the value of 2000 s^{-1} upraised the left side of the curve. Based on these test simulations the value of 200 s^{-1} was chosen for this undetermined value.

4.2 Simulation software

4.2.1 GENESIS/Kinetikit

GENESIS (GEneral NEural SImulation System) (Bower and Beeman, 1998) is a simulation environment which can be extended with graphical user interface called Kinetikit (Bhalla and Iyengar, 1999; Bhalla, 2002). GENESIS is available for downloading at http://www.genesis-sim.org/GENESIS/ and Kinetikit at http://www.ncbs.res.in/~bhalla/kkit/. GENESIS/Kinetikit can be used to model and simulate the behavior of molecular networks and pathways. In this work, GENESIS version 2.2.1 for Cygwin and Kinetikit version 10 were used. Simulations were run in Cygwin environment (Cygwin, 2006) installed on Windows XP on laptop with Pentium 4 processor. GENESIS/Kinetikit was used to obtain deterministic simulation results.

In GENESIS/Kinetikit a model is defined using different entities, for example *kpool* for reactants, such as molecules and ions, and *kreac* for reactions. In addition to modeling molecular interactions with the law of mass action (see Section 2.5), it is also possible to model ligand-gated channel activity, enzyme reactions with Michaelis-Menten kinetics, or intracellular transport process. In this work, the used IP_3R models are based on the law of mass action. Based on this law, the rates of the reactions are determined with differential equations as described in Section 2.5. In GENESIS/Kinetikit the differential equation system defined based on the model is numerically solved (simulated) as a default with Exponential Euler method (Bower and Beeman, 1998). There are also other methods available, but they were not used in this work. It is assumed that is constantly considered as well-mixed.

4.2.2 STEPS

STEPS (STochastic Engine for Pathway Simulation) (Wils and De Schutter, 2005; Wils and De Schutter, 2006) is a software created by Stefan Wils in the Theoretical Neurobiology unit, University of Antwerp, Belgium. The software can be used to numerically simulate molecular pathways and diffusion in three dimensions. STEPS extends Gillespie stochastic simulations algorithm (SSA) (Gillespie, 1976; Gillespie, 1977) for simulation of reactions and diffusion. In this work, STEPS developmental version 0.1.3 was used. Simulations were run both in computer cluster containing 2 x 2 GHz processors and in Cygwin environment (Cygwin, 2006) installed on Windows XP on laptop with Pentium 4 processor. The author of this work is the first researcher to use the software, in addition to its developer, Stefan Wils.

In STEPS, a model is described using specific markup language (STEPSML) based on XML grammar (see example in Appendix A). Use of SSA requires that all reactions are defined as one-way. For this reason forward and backward parts of reversible reactions are defined as two separate reactions in STEPS input file. The reaction constants of each reaction are given as the same rate constant values (k_f or k_b, units: 1/Ms or 1/s) as in the deterministic simulator and they are transformed to reaction probability (unit: 1/s) in STEPS. In this early version of the software, geometry and compartments of the modeled system are defined with cubes or spheres which are discretized in small cubic units or voxels. Size of a voxel (resolution, length of an edge) has to be defined by the user when describing the model using STEPSML. In STEPS, the chemical species, for example molecules or ions, are distributed evenly within a voxel and different voxels can have different amounts of chemical species. Because the geometry of a system is defined with voxels, it is possible to define walls or surfaces between voxels that belong to different compartments. This enables the use of surface bound molecules like ion channels in their natural location.

4.3 Simulations

4.3.1 Open probability of IP_3 receptor

It has been experimentally shown that the open probability of IP_3R is dependent on cytosolic Ca^{2+} concentration (Bezprozvanny et al., 1991). The dependence is bell-shaped with logarithmic x-axis. Originally, both models were built to reproduce this dependency. To verify that the models have been implemented correctly and that STEPS works properly (since the author of this work was the first user) the open probability curves were reproduced for the chosen models (Fraiman and Dawson, 2004a; Doi et al., 2005). Open probability is the proportion of open receptors of all receptors.

In the open probability simulations, the functionality of one IP_3R is simulated in constant environment until steady-state is achieved. Ca^{2+} flux through an open IP_3R is not taken into account in these simulations to maintain constant concentration for IP_3 and Ca^{2+}. The used volume of cytosol was 0.1 μm^3 (= 0.1 fl), which is an experimentally defined average volume for Purkinje cell spine (Harris and Stevens, 1988). This value was used in both deterministic and stochastic simulations. In stochastic simulations using STEPS, cytosol and ER were modeled as two cubes with volume of 0.1 μm^3 (see Figure 4.4). A resolution of 0.4642 μm was used and therefore one cube represents one voxel. Diffusion was not taken into account. When simulating the IP_3R model of Doi et al. (2005), the Ca^{2+} concentration inside the ER was ignored, because in this model IP_3R is only binding cytosolic Ca^{2+}.

The initial conditions used in open probability simulations are given in Table 4.3. The 10 μM concentration for IP_3 was chosen because the same value was used in both original papers (Fraiman and Dawson, 2004a; Doi et al., 2005). In deterministic simulations using GENESIS/Kinetikit the models were simulated with time step of 1 μs until the steady-state was achieved (either 5 s or 15 s). Simulations took a few minutes on laptop with Pentium 4 processor. The open probability of IP_3R was obtained at the end of simulation for different Ca^{2+} concentrations. In GENESIS/Kinetikit, the open probability is obtained directly as the number of open receptors.

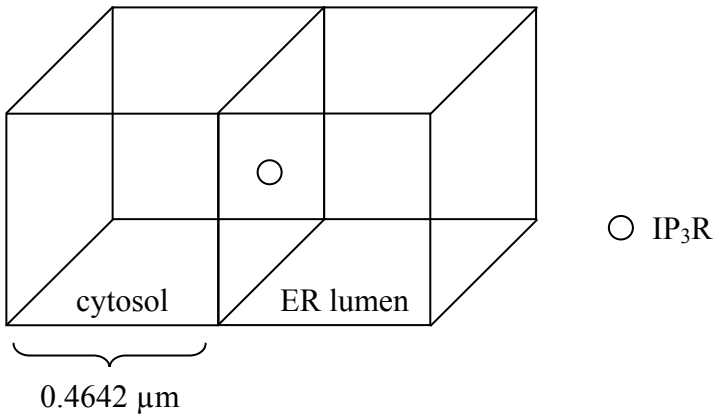

Figure 4.4. *Geometry of model in simulations with STEPS. Cytosol and ER lumen in spine were modeled as cubes (volume 0.1 µm^3). IP$_3$R is located on ER.*

Table 4.3. *Initial conditions for open probability simulations of IP$_3$R models.*

	Model	
	Doi et al. (2005)	Fraiman and Dawson (2004)
Number of IP$_3$Rs (naïve state)	1	1
[IP$_3$]	10 µM	10µM
$[Ca^{2+}]_{cyt}$	0.01 µM, 0.05 µM, 0.10 µM, 0.15 µM, 0.20 µM, 0.25 µM, 0.30 µM, 0.40 µM, 0.50 µM, 1.00 µM, 1.50 µM, 2.00 µM, 2.50 µM, 5.00 µM	0.01 µM, 0.03 µM, 0.10 µM, 0.30 µM, 0.50 µM, 0.80 µM, 1.00 µM, 1.50 µM, 3.00 µM, 10.0 µM, 30.0 µM, 100.0 µM
$[Ca^{2+}]_{ER}$	-	150 µM
Other states of IP$_3$R	0	0

In stochastic simulations with STEPS the models were simulated for 20 s using a sampling frequency of 0.1 s. For each initial Ca^{2+} concentration, the open probability was calculated as an average of the open IP$_3$Rs from a period of 10-20 s and 100 simulations. In stochastic simulations the steady-state was achieved before 10 s time. It took few minutes to perform 100 simulations on the used cluster computer.

4.3.2 Dynamic behavior of IP_3 receptor

A cell is a constantly changing, dynamic system and it is therefore important to study the dynamic behavior of intracellular functions in addition to steady-state research. In this work the dynamic behavior of IP_3R models was studied by following cytosolic Ca^{2+} concentration as a function of time. These simulations were done for both IP_3R models (Fraiman and Dawson, 2004a; Doi et al., 2005).

In the dynamic simulations, the Ca^{2+} flux through the open IP_3Rs was modeled in addition to IP_3R state transitions. In GENESIS/Kinetikit, flux is modeled using *kchan* entity which describes ligand-gated channel. The equation for flux behind *kchan* is not published, but the rate of the flux is controlled with parameter defined by a user. In STEPS the flux is dependent on the concentrations of the flowing species on the different sides of membrane. The equation used in STEPS is the following

$$\frac{\mathrm{d}[\mathrm{B}]_{\mathrm{out}}}{\mathrm{d}t} = -\frac{\mathrm{d}[\mathrm{B}]_{\mathrm{in}}}{\mathrm{d}t} = \frac{k}{VN_A}([\mathrm{B}]_{\mathrm{in}} - [\mathrm{B}]_{\mathrm{out}}),\ \text{when}\ [\mathrm{B}]_{\mathrm{in}} - [\mathrm{B}]_{\mathrm{out}} > 0,\ \text{otherwise}\ 0 \qquad (4.1)$$

where B is the species going through the open channel, *k* is the rate parameter, V is the volume of a voxel, and N_A the Avogadro's number. Although the basic equation is deterministic, it is simulated in stochastic matter as all the reactions in STEPS. Based on test simulations (results not shown) the equation for the flux in GENESIS/Kinetikit is almost the same as in STEPS.

Rate parameters were estimated for both simulators separately. The estimation was done based on experimental data by Bezprozvanny and Ehrlich (1994). It is estimated that a number of 5400 Ca^{2+} ions goes though open IP_3R during one opening and that mean open time of IP_3R is 3.7 ms (Bezprozvanny and Ehrlich, 1994). The estimated parameter values for flux functions were for 595 (unit not given) for GENESIS/Kinetikit and $5.8*10^8$ $M^{-1}s^{-1}$ for STEPS.

Dynamic simulations were done with identical geometry and volume as open probability simulations (see Figure 4.4). Diffusion was not taken into account in these simulations either. In these simulations, the concentration of the cytosolic Ca^{2+} was

followed as a function of time. The initial conditions used in dynamic simulations are given in Table 4.4. The average number of IP_3Rs in a Purkinje cell spine has been estimated to be 16 (see Supplemental material of Doi et al., 2005). There are five different initial concentrations for IP_3 and six for cytosolic Ca^{2+}. All combinations of the initial concentrations were used in simulations. Therefore, both models were simulated using altogether 30 different conditions once in GENESIS/Kinetikit (30 simulation results) and 100 times in STEPS (3000 simulation results). STEPS produces automatically files containing the number of Ca^{2+} in different time point and from GENESIS/Kinetikit this information have to be exported.

Table 4.4. *Initial conditions for dynamic simulations of the IP_3R models.*

Species	Value
Number of IP_3Rs (naïve state)	16
$[IP_3]$	0.1 μM, 0.2 μM, 0.5 μM, 1.0 μM, 5.0 μM
$[Ca^{2+}]_{cyt}$	0.01 μM, 0.05 μM, 0.1 μM, 0.2 μM, 0.5 μM, 1 μM
$[Ca^{2+}]_{ER}$	150 μM
Other states of IP_3R	0

4.4 Data analysis

Due to the fact that large sets of simulation data were obtained in this work, the analysis of the data was done using MATLAB® programming environment. The data points of deterministic open probability simulations were manually imported to MATLAB®. There is one open probability value for each cytosolic Ca^{2+} concentrations for both models (concentrations in Table 4.3). The data related to stochastic open probability simulations were in text files each containing two columns, time points from 10 s to 20 s and the number of open IP_3Rs for each time point. There were 100 simulation replicates and thus 100 files (one open state) from simulations with the model of Doi et al. (2005) and 300 files (three open states) from simulations with the model of Fraiman and Dawson (2004a) for each cytosolic Ca^{2+} concentration value. The data from these files was imported to MATLAB® using a script. A script is a sequence of commands that can also include programming statements, for example *if* statements or *for* loops.

The number of open IP_3Rs from the simulations with the model of Fraiman and Dawson (2004a) in different open states were summed. A mean value of the number of open IP_3Rs in each file or for the sum of three files was calculated. These mean values for each Ca^{2+} concentration were arranged to a matrix to make the handling of the data more straightforward. The error was calculated as a standard deviation of the means of the replicates. The open probability was calculated as an average of the means for the 100 simulations. The error in stochastic simulations was calculated as a standard deviation of the 10-20 s averages for 100 simulations. The calculated mean values and errors were plotted in the same figure with the deterministic results.

Results from dynamic simulations were also imported to MATLAB® using a script. There were one deterministic result and 100 replicates from stochastic simulations for each pair of initial concentrations of IP_3 and cytosolic Ca^{2+}. This data was arranged in a matrix where the first column contained time and the others contained the amounts of Ca^{2+}. The amounts of Ca^{2+} were transformed to concentrations and averages of the replicates were calculated. The deterministic result was plotted among the 100 stochastic replicates and the average of replicates in the same figure. The deterministic and stochastic results were compared in two different ways: (1) by plotting the maximum Ca^{2+} concentration and (2) by comparing the time points where half of the maximum Ca^{2+} concentration in cytosol was reached. The values of maximum concentration and the time points were obtained by going through the data matrices using a script. The maximum Ca^{2+} concentration and the time points were plotted as surface plots against initial concentrations of cytosolic Ca^{2+} and IP_3 separately for deterministic and stochastic simulations.

5 Results

5.1 Open probability of IP_3 receptor

Open probability simulations were done to verify that the models have been implemented correctly. Open probability curves of IP_3 receptor (IP_3R) were simulated for the selected IP_3R models (Fraiman and Dawson, 2004a; Doi et al., 2005) using GENESIS/Kinetikit (Bower and Beeman, 1998; Bhalla and Iyengar, 1999; Bhalla, 2002) and STEPS (Wils and De Schutter, 2005). The curves represent the open probability of IP_3R (y-axes) as a function of cytosolic Ca^{2+} concentration (x-axes) (shown in Figure 5.1). The open probability curves obtained from deterministic (GENESIS/Kinetikit) and stochastic (STEPS) simulations are consistent with both models as expected.

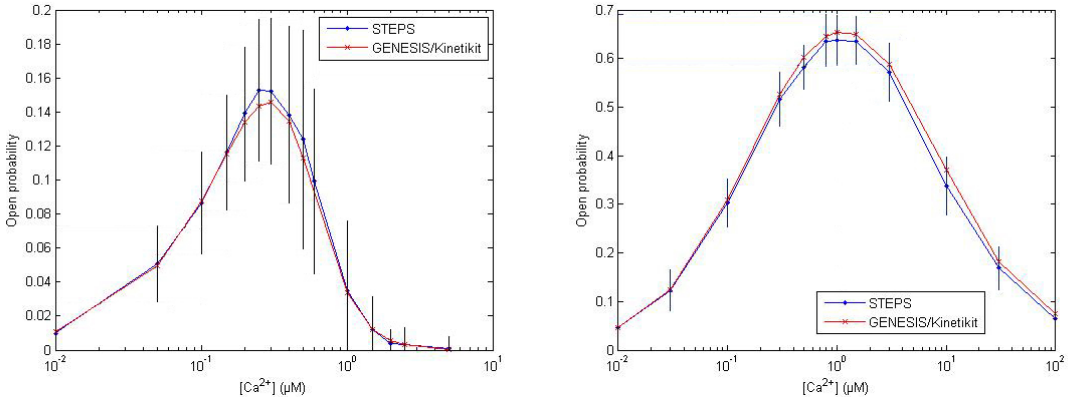

Figure 5.1. *Open probability curves of the IP_3R model of Doi et al. (2005) (left) and Fraiman and Dawson (2004) (right). The deterministic (red) and stochastic (blue) curves are in agreement for both models. Every point in stochastic simulations represents an average of 100 independent simulations. Standard deviation of stochastic simulation results are shown as black error bars. The y-axes have arbitrary scale.*

5.2 Dynamic behavior of IP_3 receptor

To study the dynamic behavior of the two IP_3R models, cytosolic Ca^{2+} concentration was followed as a function of time. The models were simulated by varying the initial

concentrations of IP_3 and cytosolic Ca^{2+} (values given in Table 4.4) to see how the Ca^{2+} concentration evolves in different conditions. Altogether, 30 different combinations of concentrations were used. One deterministic simulation response and 100 stochastic simulation responses were obtained for each combination. Examples of simulation results with both IP_3R models are shown in Figures 5.2 and 5.3.

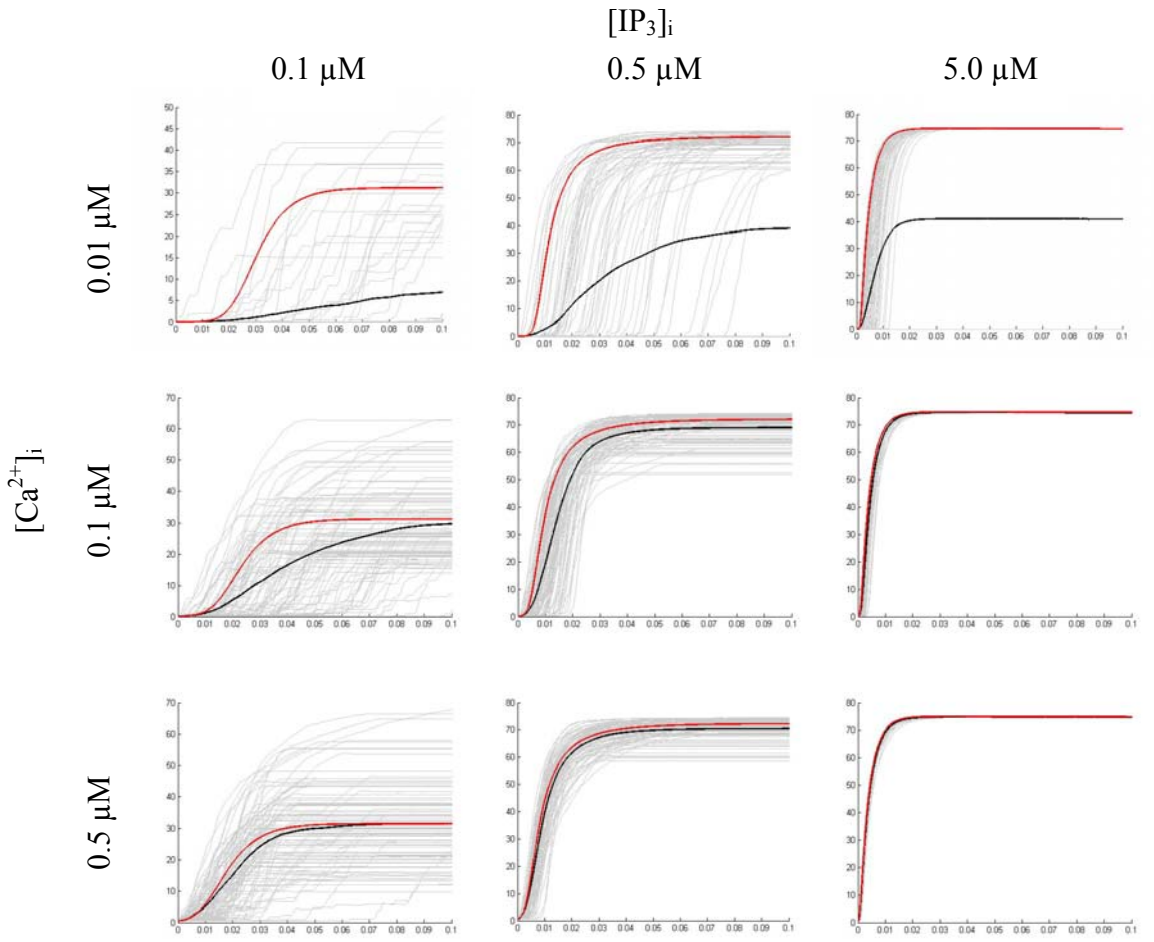

Figure 5.2. *Dynamic simulation results obtained with IP_3R model of Doi et al. (2005). Cytosolic $[Ca^{2+}]$ (in μM, on the y-axes) is presented as a function of time in seconds (x-axes). Results from deterministic (red) and stochastic (grey) simulations, and the mean value (black) of 100 stochastic simulations are shown. Initial values for $[IP_3]$ (on the top) and cytosolic $[Ca^{2+}]$ (on the left) are given for each subplot.*

Each subfigure in Figure 5.2 and 5.3 includes the deterministic result, 100 stochastic results, and the average of the stochastic results. As can be seen from the figures the variation in stochastic simulations increases when initial IP_3 and Ca^{2+} concentrations decrease. More specifically, this can be seen by looking at the variability among grey lines in Figures 5.2 and 5.3. Individual stochastic curves (grey) also have more step-like

or rough behavior compared to very smooth deterministic ones. The most significant finding in these simulations is that there is a difference in the maximum values and the slopes of the curves between the average of stochastic simulation results (black in Figures 5.2 and 5.3) and the deterministic results (red) with small initial concentrations. These results are similar with both models.

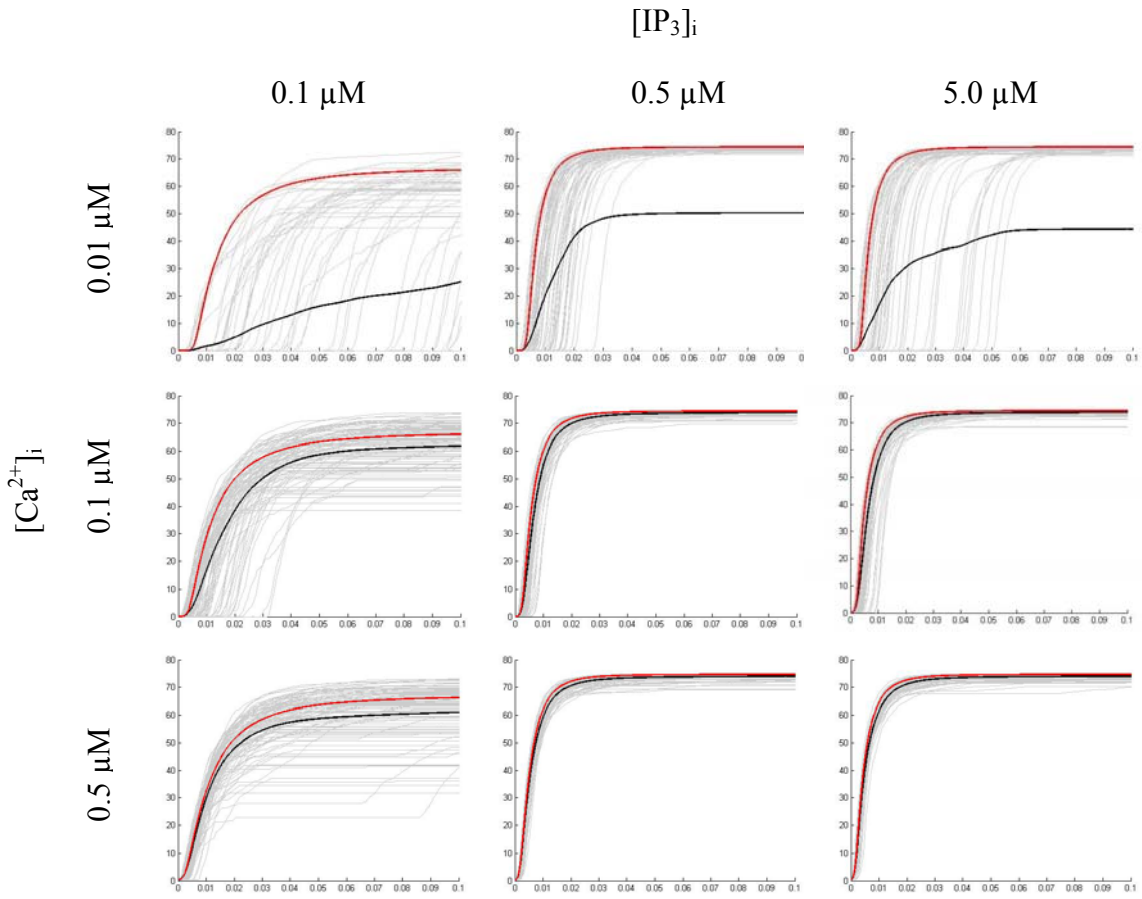

Figure 5.3. *Dynamic simulation results obtained with IP_3R model of Fraiman and Dawson (2004). Cytosolic $[Ca^{2+}]$ (in µM, on the y-axes) is presented as a function of time (in seconds, x-axes). Results from deterministic (red) and stochastic (grey) simulations, and mean value (black) of 100 stochastic simulations are shown. Initial values for $[IP_3]$ (on the top) and cytosolic $[Ca^{2+}]$ (on the left) are given for each subplot.*

To further understand the behavior of cytosolic Ca^{2+} concentration, two different parameters were examined. First, the maximum Ca^{2+} concentration reached during simulations was measured as a function of the initial IP_3 and initial cytosolic Ca^{2+} concentrations (Figures 5.4 (Doi et al.) and 5.5 (Fraiman and Dawson)) because of the differences between deterministic and stochastic simulation results. The plots were drawn for both deterministic and stochastic (mean curve of 100 simulations) simulation

results. Second, the time at which half of the maximum cytosolic Ca^{2+} concentration was reached was measured as a function of the initial IP_3 and initial cytosolic Ca^{2+} concentrations (Figures 5.6 and 5.7). This is an easy way to compare the slopes of the curves at the steepest region. The slope tells here how fast the concentration changes.

The surface plots in Figures 5.4 and 5.5 show that the maximum cytosolic Ca^{2+} concentration attained in the deterministic simulations with both models is dependent only on initial IP_3 concentration, not on initial Ca^{2+} concentration. The latter might be due to the quick response to rising Ca^{2+} concentration. Ca^{2+} concentration rises when the channel opens and so the initial concentration does not have much effect on the maximum concentration at least in this case where the rate of Ca^{2+} release behaves similarly in all cases. In the stochastic simulations the results are similar to the deterministic ones above initial cytosolic Ca^{2+}concentration of 0.1 µM. Below this concentration value, the maximum Ca^{2+} concentration is also dependent on the initial Ca^{2+} concentration. The Ca^{2+} concentration stays at 0 and IP_3R does not always open in these conditions. This can be seen, for example, in the right top subplot in Figure 5.2, where some of the stochastic results (grey) are near the deterministic one (red) or remain at 0. This concentration threshold is the same for both models.

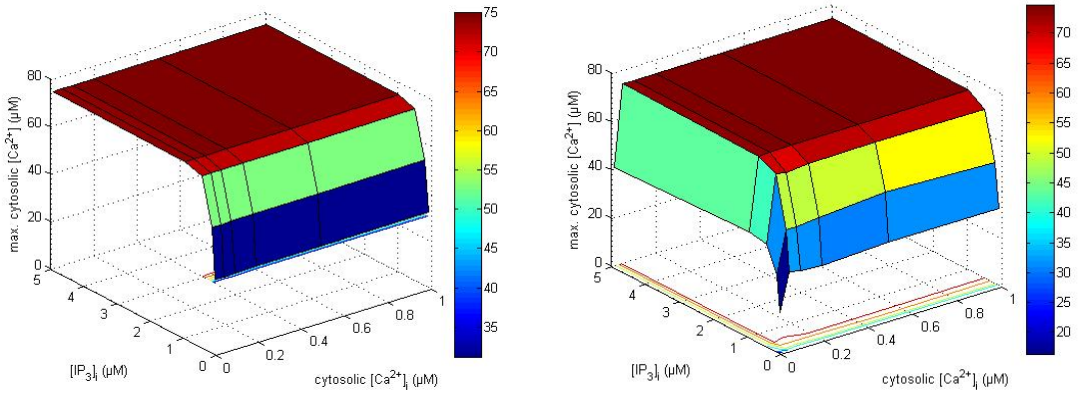

Figure 5.4. *Maximum cytosolic [Ca^{2+}] as a function of initial [IP_3] and initial cytosolic [Ca^{2+}] in simulations with IP_3R model of Doi et al. (2005). Results from the deterministic simulations are shown on the left and from the stochastic ones on the right. The color scale emphasizes the values on z-axes.*

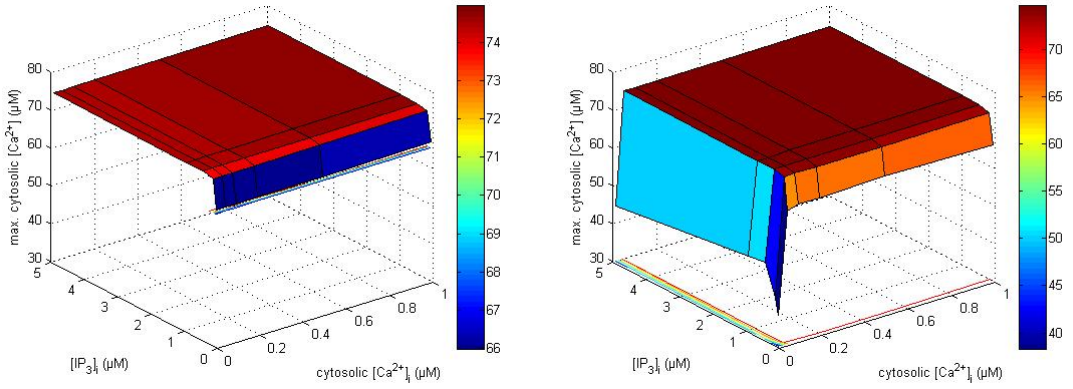

Figure 5.5. *Maximum cytosolic [Ca^{2+}] as a function of initial [IP_3] and initial cytosolic [Ca^{2+}] in simulations with IP_3R model of Fraiman and Dawson (2004). Results from the deterministic simulations are shown on the left and from the stochastic ones on the right.*

The time at which half of the maximum cytosolic Ca^{2+} concentration was reached is dependent on the initial IP_3 concentration in deterministic and stochastic simulations (see Figures 5.6 and 5.7). However, in deterministic simulations, minor dependence on the initial Ca^{2+} can be seen, whereas, in stochastic simulations, dependence on the initial Ca^{2+} is more pronounced. In stochastic simulations the dependence on both IP_3 and Ca^{2+} is evidently seen as a peak in the plots. These results are consistent with both models.

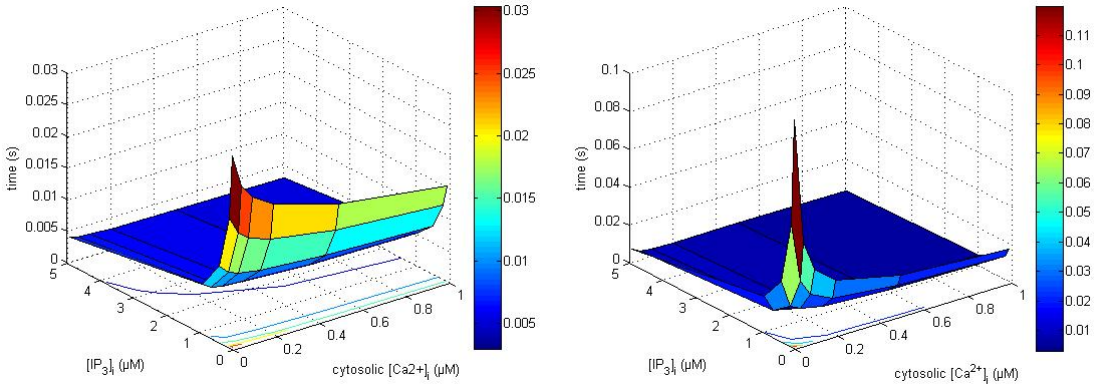

Figure 5.6. *Time at which half of the maximum cytosolic [Ca^{2+}] was reached as a function of initial [IP_3] and initial cytosolic [Ca^{2+}] in simulations with IP_3R model of Doi et al. (2005). Results from the deterministic simulations are on the left and from the stochastic ones on the right. Notice the difference on z-axes scales.*

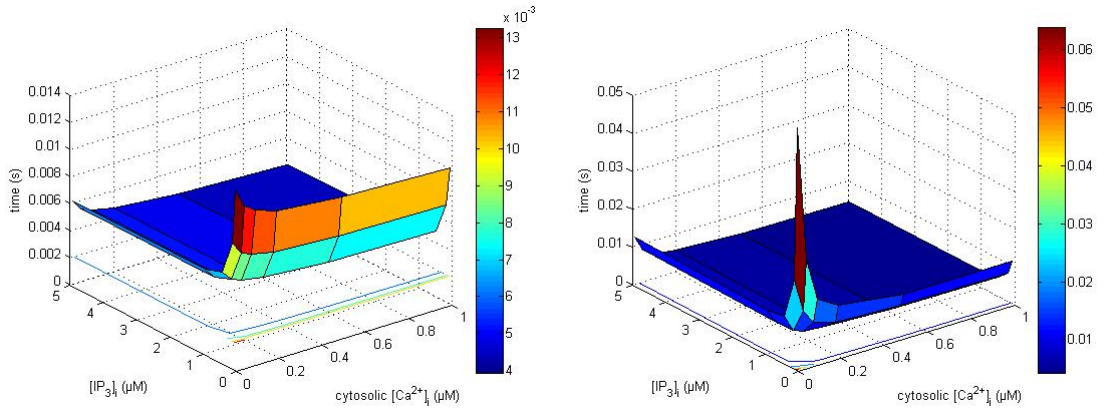

Figure 5.7. *Time at which half of the maximum cytosolic [Ca^{2+}] was reached as a function of initial [IP_3] and initial cytosolic [Ca^{2+}] in simulations with IP_3R model of Fraiman and Dawson (2004). Results from the deterministic simulations are on the left and from the stochastic ones on right. Notice the difference on z-axes scales.*

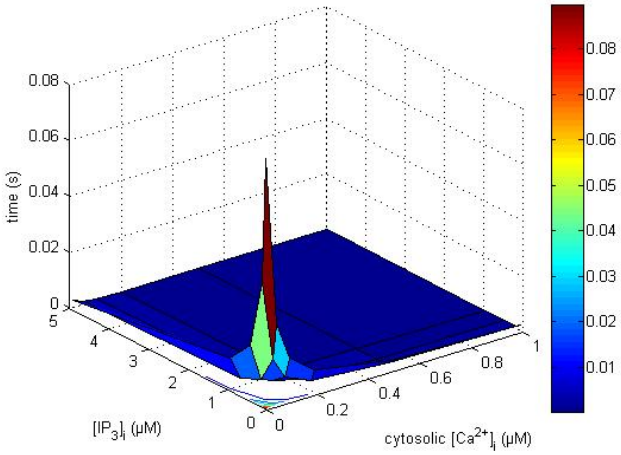

Figure 5.8. *Difference between deterministic and stochastic results represented in Figure 5.6.*

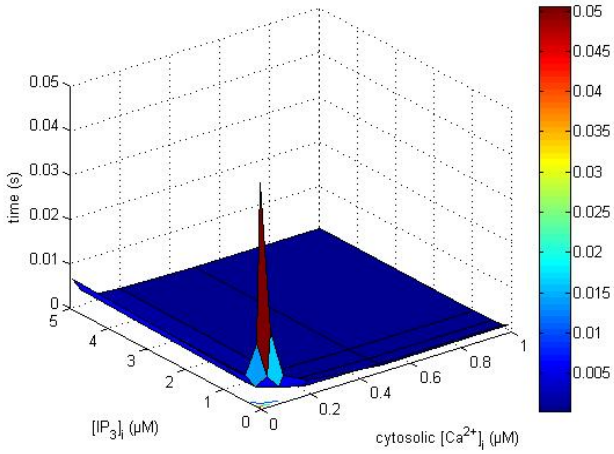

Figure 5.9*. Difference between deterministic and stochastic results represented in Figure 5.7.*

To study the difference between deterministic and stochastic simulation results in times at which half of the maximum cytosolic Ca^{2+} concentration was reached the deterministic plots were subtracted from the stochastic plots of both models. These differences are shown in Figures 5.8 and 5.9. It can bee seen that there is a difference between deterministic and stochastic simulation results. Furthermore, a threshold, below which the effect of stochasticity becomes significant, can be determined from these plots. In the case of IP_3R model of Doi et al. (2005) the thresholds for initial IP_3 concentration is 0.5 μM - 1.0 μM and for initial cytosolic Ca^{2+} concentration 0.2 μM - 0.1 μM. In the case of IP_3R model of Fraiman and Dawson (2004a) the thresholds are slightly lower, for IP_3 0.5 μM and for Ca^{2+} 0.1 μM. This difference will be discussed in the Section 6.3.

6 Discussion

In addition to traditional experimental research in molecular biology, computational study of intracellular systems is important to fully understand the complex processes occurring in the cell. Using mathematical modeling and simulation, it is possible to describe and analyze the dynamic behavior of a biological system. The models should be constructed and simulations run so that the experimental data is reproduced correctly and also prediction of other behavior can be made. In the following, the implications of model structures and simulators on the obtained results are discussed in more detail.

6.1 Models

The structures of both models (Fraiman and Dawson, 2004a; Doi et al., 2005) that were used as test cases are relatively simple. In general, both models are good representatives for IP_3 receptor function although they contain some inconsistencies compared to experimental findings. In both cases, IP_3 receptor has four subunits, but in neither of them the receptor has the four binding sites for IP_3 suggested by Taylor et al. (2004). The sequential binding of IP_3 and Ca^{2+} leading to an opening of an ion channel has been proposed to be a characteristic feature of the IP_3 receptor (Taylor et al., 2004; Sneyd and Falcke, 2005). In this work, both models require the sequential binding for opening an ion channel.

Only three of the original six open states in the model of Fraiman and Dawson (2004a) were considered as open in this work. In the original work of Fraiman and Dawson (2004a) the states had been included to reproduce the spontaneous activity of IP_3R in the absence of IP_3 and when the Ca^{2+} concentration was below 5 nM (Mak et al., 2003; Fraiman and Dawson, 2004a). In this work, this was done to simplify the model and to reduce the amount of data. The simplification of the model was found not change the open probability curve and thus have no significant impact on the results. Also, the concentrations used in this work are higher so that it even should not have any effect. At least in STEPS, the model for Ca^{2+} flux depends only on the Ca^{2+} concentration on both

sides of the membrane (see Equation 4.1) while in reality it depends on both the concentration difference and electrical interactions.

6.2 Simulation software

Installation of GENESIS/Kinetikit (Bower and Beeman, 1998; Bhalla and Iyengar, 1999; Bhalla, 2002) to Cygwin on Windows was slightly difficult even for a person having knowledge on UNIX and Linux operating systems. The relatively simple structure of the models made implementation quite straightforward. The implementation of the models to GENESIS/Kinetikit was more laborious than to STEPS (Wils and De Schutter, 2005), although GENESIS/Kinetikit has a graphical user interface (GUI). The GUI of GENESIS/Kinetikit is not always logical. One major drawback in it was that when a model was constructed and then opened again some arrows representing the reactions were not shown. This caused inconvenience especially when the implementation was not ready.

Because a developmental version of STEPS was used in this study the most difficult part using the software was the installation. On the other hand, it was relatively easy to use STEPS after having familiarized with the markup language, STEPSML, used for describing the model (see Appendix 1 for an example). In STEPS, but not in GENESIS/Kinetikit, it is possible to take the diffusion of molecules and ions into account. However, this option was not used so that the simulation results would be more comparable. The effects of diffusion will be included in our future studies.

6.3 Significance of results

Both models produced the bell-shaped open probability curves (see Figure 5.1). The open probability simulations were performed to ensure that the models were implemented correctly. The curves were compared to those in the original papers (Fraiman and Dawson, 2004a; Doi et al., 2005) and they were similar. The curve of the model of Doi et al. (2005) is not as symmetrical as the experimentally obtained curve. There is also a difference in the Ca^{2+} concentration where the maximal open probability

is reached: it is about 1-1.5 μM in the model Fraiman and Dawson (2004a) when with the model of Doi et al. (2005) it is approximately 0.3 μM. The concentration of IP_3 (10 μM) was the same in simulations with both models and thus the maxima should have been identical if the models were working similarly. Experimental work has shown that the maximum open probability for IP_3 receptor isolated from cerebellum and for recombinant type 1 IP_3 receptor are attained for Ca^{2+} concentration of 0.2 μM (Bezprozvanny et al., 1991) and 0.15 μM (Kaznacheyeva et al., 1998) when the concentration of IP_3 is 2 μM. These Ca^{2+} concentration values for maximum open probability cannot be used for direct comparison because of the different IP_3 concentration.

The dynamic simulations were done to study the time series behavior of IP_3 receptor and Ca^{2+} release. The results from these simulations were analyzed by taking a look at some of their characteristics, maximum Ca^{2+} concentration, and the time at which half of the maximum Ca^{2+} concentration was reached. These characteristics are presented as figures instead of numbers to make them more illustrative. Some additional characteristics like variance or CV (coefficient of variation; standard deviation divided by mean) related to the results obtained by stochastic simulations could have been determined. However, figures were considered to be sufficient enough for comparison of deterministic and stochastic results. The amount of replicates could have been slightly higher but it was limited to 100 so that the simulations and the analysis could be done in reasonable time. 100 replicates were found to be adequate for comparative analysis of stochastic replicates in this work.

The results of this Master's thesis indicate that there is a difference in deterministic and stochastic simulations below certain thresholds of initial concentrations of cytosolic Ca^{2+} and IP_3. In the case of IP_3 receptor model of Doi et al. (2005) the threshold for initial IP_3 concentration is 0.5 μM – 1.0 μM and for initial cytosolic Ca^{2+} concentration 0.2 μM - 0.1 μM. For the IP_3 receptor model of Fraiman and Dawson (2004a) the thresholds are slightly lower, for IP_3 0.5 μM and for Ca^{2+} 0.1 μM. The thresholds for Ca^{2+} are close to the resting level of Ca^{2+} concentration, 70 ± 29 nM, determined in spines of hippocampal pyramidal neuron (Sabatini et al., 2002).

The difference in the thresholds between the two models might be due to different dynamic responses to changes in Ca^{2+} concentration. This indicates that there are different threshold for different models. Turner et al. (2004) reported that they did not obtain significant difference between deterministic and stochastic simulations of a model with Michaelis-Menten mechanism and 100 molecules. With the volume used in this work, 100 molecules correspond to a concentration of 1 μM. The threshold for significant effects of stochasticity is about 1 μM for IP_3 but the threshold for Ca^{2+} is much lower. Our work then implies that there is a difference when having 100 or less molecules. Even though the mean of 100 stochastic simulations are consistent with the deterministic simulation results in larger concentrations, the variation in stochastic results (see grey lines in Figures 5.2 and 5.3) might have a biologically important role. The stochastic approaches should be used at least below these thresholds to achieve realistic results.

In general, models should be structurally and functionally as realistic as possible, although the simulation time increases with the level of details. Because the stochastic approaches are computationally more expensive than the deterministic ones, a usage of hybrids of these approaches should be also considered. This way more realistic results could be obtained and the simulation time might not become infeasible. Compartmental and spatial modeling should be used more often because reactions are local in most cases. The cell includes different organelles and membranes, the concentrations of molecules and ions vary through the cell, and large amount of proteins are membrane-bound or expressed only in certain membranes. In future, the effects of diffusion and different spatial distributions of IP_3 receptors need to be studied. The present work sets a foundation for developing structurally and functionally more relevant models for IP_3 receptor to reproduce correct time series behavior.

7 Conclusions

In this work, the importance of stochasticity in simulation of IP_3 receptor function was examined. Based on the literature review two mathematical models of IP_3 receptor were selected as test cases: the IP_3 receptor model of Doi et al. (2005) and the model of Fraiman and Dawson (2004a). Based on dynamic simulation results of both models, I have shown that there exists a threshold for initial IP_3 and cytosolic Ca^{2+} concentrations below which the effect of stochasticity in reaction kinetics becomes meaningful. The threshold for Ca^{2+} concentration is close to the resting level of Ca^{2+} concentration in spines and thus it corresponds to the resting state of a spine before Ca^{2+} signals are induced. The present study implies that the models of IP_3 receptor need to be studied more thoroughly before they can be used in stochastic simulations of Ca^{2+} dynamics synaptic plasticity. The need for stochastic modeling and simulation methods is clearly evident in specific situations when small molecular concentrations are involved. Instead of using deterministic approaches more efforts should be directed towards stochastic modeling and simulation of cell and molecular biological phenomena.

References

Adkins CE, Taylor CW. Lateral inhibition of inositol 1,4,5-trisphosphate receptors by cytosolic Ca(2+). Curr.Biol. 1999;9:1115-1118.

Alberts B, Johnson A, Lewis J, Raff M, Roberts K, Walter P. Molecular biology of the cell, Garland Science, New York, USA, 2002, pp. 831-906.

Apps R, Garwicz M. Anatomical and physiological foundations of cerebellar information processing. Nat.Rev.Neurosci. 2005;6:297-311.

Atri A, Amundson J, Clapham D, Sneyd J. A single-pool model for intracellular calcium oscillations and waves in the Xenopus laevis oocyte. Biophys.J. 1993;65:1727-1739.

Augustine GJ, Santamaria F, Tanaka K. Local calcium signaling in neurons. Neuron 2003;40:331-346.

Banerjee S, Hasan G. The InsP3 receptor: its role in neuronal physiology and neurodegeneration. Bioessays 2005;27:1035-1047.

Barbour B. Synaptic currents evoked in Purkinje cells by stimulating individual granule cells. Neuron 1993;11:759-769.

Bezprozvanny I. Theoretical analysis of calcium wave propagation based on inositol (1,4,5)-trisphosphate (InsP3) receptor functional properties. Cell Calcium 1994;16:151-166.

Bezprozvanny I, Ehrlich BE. Inositol (1,4,5)-trisphosphate (InsP3)-gated Ca channels from cerebellum: conduction properties for divalent cations and regulation by intraluminal calcium. J.Gen.Physiol. 1994;104:821-856.

Bezprozvanny I, Watras J, Ehrlich BE. Bell-shaped calcium-response curves of Ins(1,4,5)P3- and calcium-gated channels from endoplasmic reticulum of cerebellum. Nature 1991;351:751-754.

Bhalla US. Use of Kinetikit and GENESIS for modeling signaling pathways. Methods Enzymol. 2002;345:3-23.

Bhalla US. Signaling in small subcellular volumes. I. Stochastic and diffusion effects on individual pathways. Biophys.J. 2004a;87:733-744.

Bhalla US. Signaling in small subcellular volumes. II. Stochastic and diffusion effects on synaptic network properties. Biophys.J. 2004b;87:745-753.

Bhalla US, Iyengar R. Emergent properties of networks of biological signaling pathways. Science 1999;283:381-387.

Bloedel JR. Functional heterogeneity with structural homogeneity**:** How does the cerebellum operate? Behav.Brain Sci. 1992;15:666-678.

Bootman MD, Lipp P. Ringing changes to the 'bell-shaped curve'. Curr.Biol. 1999;9:R876-878.

Bower JM, Beeman D. The book of GENESIS: Exploring realistic neural models with the GEneral NEural SImulation System, Springer-Verlag, New York, 1998.

Copeland RA. Enzymes: a practical introduction to structure, mechanism, and data analysis, Wiley-VCH, New York, USA, 2000, pp. 36-41.

Cygwin. http://www.cygwin.com/ [accessed: 7 September 2006].

Dawson AP, Lea EJ, Irvine RF. Kinetic model of the inositol trisphosphate receptor that shows both steady-state and quantal patterns of Ca2+ release from intracellular stores. Biochem.J. 2003;370:621-629.

De Young GW, Keizer J. A single-pool inositol 1,4,5-trisphosphate-receptor-based model for agonist-stimulated oscillations in Ca2+ concentration. Proc.Natl.Acad.Sci. U.S.A. 1992;89:9895-9899.

Diambra L, Guisoni N. Modeling stochastic Ca2+ release from a cluster of IP3-sensitive receptors. Cell Calcium 2005;37:321-332.

Doi T, Kuroda S, Michikawa T, Kawato M. Inositol 1,4,5-trisphosphate-dependent Ca2+ threshold dynamics detect spike timing in cerebellar Purkinje cells. J.Neurosci. 2005;25:950-961. Neuroscience online, URL http://www.jneurosci.org/

Ekerot CF, Kano M. Long-term depression of parallel fibre synapses following stimulation of climbing fibres. Brain Res. 1985;342:357-360.

Eldén L, Wittmeyer-Koch L, Nielsen HB. Introduction to numerical computation: analysis and MATLAB illustrations, Studentlitteratur, Lund, 2004, pp. 309-358.

Falcke M. On the role of stochastic channel behavior in intracellular Ca2+ dynamics. Biophys.J. 2003;84:42-56.

Fraiman D, Dawson SP. A model of IP3 receptor with a luminal calcium binding site: stochastic simulations and analysis. Cell Calcium 2004a;35:403-413.

Fraiman D, Dawson SP. Erratum to "A model of the IP3 receptor with a luminal calcium binding site: stochastic simulation and analysis". Cell Calcium 2004b;36:445.

Ghez C, Thach WT. Cerebellum. In: Kandel ER, Schwartz JH and Jessel TM (eds), Principles of neural science, McGraw-Hill, U.S.A., 2000, pp. 832-852.

Gillespie DT. A general method for numerical simulating the stochastic time evolution of coupled chemical reactions. J.Comp.Phys. 1976;22:403-434.

Gillespie DT. Exact stochastic simulation of coupled chemical reactions. J.Phys.Chem. 1977;81:2340-2361.

Haeri HH, Hashemianzadeh SM, Monajjemi M. A kinetic Monte Carlo simulation study of inositol 1,4,5-trisphosphate receptor (IP3R) calcium release channel. Comput.Biol.Chem. 2007;31:99-109.

Hamada K, Miyata T, Mayanagi K, Hirota J, Mikoshiba K. Two-state conformational changes in inositol 1,4,5-trisphosphate receptor regulated by calcium. J.Biol.Chem. 2002;277:21115-21118.

Hamada K, Terauchi A, Mikoshiba K. Three-dimensional rearrangements within inositol 1,4,5-trisphosphate receptor by calcium. J.Biol.Chem. 2003;278:52881-52889.

Harris KM. Structure, development, and plasticity of dendritic spines. Curr.Opin.Neurobiol. 1999;9:343-348.

Harris KM, Stevens JK. Dendritic spines of rat cerebellar Purkinje cells: serial electron microscopy with reference to their biophysical characteristics. J.Neurosci. 1988;8:4455-4469.

Hering H, Sheng M. Dendritic spines: structure, dynamics and regulation. Nat.Rev.Neurosci. 2001;2:880-888.

Hituri K, Achard P, Wils S, Linne M-L, De Schutter E. Stochastic modeling of inositol-1,4,5-trisphophate receptors in Purkinje cell spine. 15th Annual Meeting of the Organization for Computational Neurosciences CNS*2006, Edinburgh, UK, July 16-20, 2006.

Iino M. Biphasic Ca2+ dependence of inositol 1,4,5-trisphosphate-induced Ca release in smooth muscle cells of the guinea pig taenia caeci. J.Gen.Physiol. 1990;95:1103-1122.

Iino M. Ca2+-dependent inositol 1,4,5-trisphosphate and nitric oxide signaling in cerebellar neurons. J.Pharmacol.Sci. 2006;100:538-544.

Ito M. Cerebellar long-term depression: characterization, signal transduction, and functional roles. Physiol.Rev. 2001;81:1143-1195.

Ito M. The molecular organization of cerebellar long-term depression. Nat.Rev.Neurosci. 2002;3:896-902.

Ito M. Cerebellar circuitry as a neuronal machine. Prog.Neurobiol. 2006;78:272-303.

Ito M, Sakurai M, Tongroach P. Climbing fibre induced depression of both mossy fibre responsiveness and glutamate sensitivity of cerebellar Purkinje cells. J.Physiol. 1982;324:113-134.

Kaftan EJ, Ehrlich BE, Watras J. Inositol 1,4,5-trisphosphate (InsP3) and calcium interact to increase the dynamic range of InsP3 receptor-dependent calcium signaling. J.Gen.Physiol. 1997;110:529-538.

Kaznacheyeva E, Lupu VD, Bezprozvanny I. Single-channel properties of inositol (1,4,5)-trisphosphate receptor heterologously expressed in HEK-293 cells. J.Gen.Physiol. 1998;111:847-856.

Kennedy MB, Beale HC, Carlisle HJ, Washburn LR. Integration of biochemical signalling in spines. Nat.Rev.Neurosci. 2005;6:423-434.

Kinetikit manual. http://www.ncbs.res.in/~bhalla/kkit/manual.html [accessed: 7 November 2006].

Konnerth A, Dreessen J, Augustine GJ. Brief dendritic calcium signals initiate long-lasting synaptic depression in cerebellar Purkinje cells. Proc.Natl.Acad.Sci.U.S.A. 1992;89:7051-7055.

Laurent M, Claret M. Signal-induced Ca2+ oscillations through the regulation of the inositol 1,4,5-trisphosphate-gated Ca2+ channel: an allosteric model. J.Theor.Biol. 1997;186:307-326.

LeBeau AP, Yule DI, Groblewski GE, Sneyd J. Agonist-dependent phosphorylation of the inositol 1,4,5-trisphosphate receptor: A possible mechanism for agonist-specific calcium oscillations in pancreatic acinar cells. J.Gen.Physiol. 1999;113:851-872.

Leckovac V. Comprehensive enzyme kinetics, Kluwer Academic/Plenum Publishers, New York, USA, 2003, pp. 11-30.

Lee KJ, Kim H, Rhyu IJ. The roles of dendritic spine shapes in Purkinje cells. Cerebellum 2005;4:97-104.

Li YX, Rinzel J. Equations for InsP3 receptor-mediated [Ca2+]i oscillations derived from a detailed kinetic model: a Hodgkin-Huxley like formalism. J.Theor.Biol. 1994;166:461-473.

Maeda N, Niinobe M, Inoue Y, Mikoshiba K. Developmental expression and intracellular location of P400 protein characteristic of Purkinje cells in the mouse cerebellum. Dev.Biol. 1989;133:67-76.

Mak DO, McBride S, Foskett JK. Regulation by Ca2+ and inositol 1,4,5-trisphosphate (InsP3) of single recombinant type 3 InsP3 receptor channels. Ca2+ activation uniquely distinguishes types 1 and 3 insp3 receptors. J.Gen.Physiol. 2001;117:435-446.

Mak DO, McBride SM, Foskett JK. Spontaneous channel activity of the inositol 1,4,5-trisphosphate (InsP3) receptor (InsP3R). Application of allosteric modeling to calcium and InsP3 regulation of InsP3R single-channel gating. J.Gen.Physiol. 2003;122:583-603.

Manninen T, Linne M-L, Ruohonen K. A novel approach to model neuronal signal transduction using stochastic differential equations. Neurocomputing 2006a;69:1066-1069.

Manninen T, Linne M-L, Ruohonen K. Developing Ito stochastic differential equation models for neuronal signal transduction pathways. Comput.Biol.Chem. 2006b;30:280-291.

Marchant JS, Taylor CW. Cooperative activation of IP3 receptors by sequential binding of IP3 and Ca2+ safeguards against spontaneous activity. Curr.Biol. 1997;7:510-518.

Means S, Smith AJ, Shepherd J, Shadid J, Fowler J, Wojcikiewicz RJ, Mazel T, Smith GD, Wilson BS. Reaction diffusion modeling of calcium dynamics with realistic ER geometry. Biophys.J. 2006;91:537-557.

Melamed-Book N, Kachalsky SG, Kaiserman I, Rahamimoff R. Neuronal calcium sparks and intracellular calcium "noise". Proc.Natl.Acad.Sci.U.S.A. 1999;96:15217-15221.

Miyata M, Finch EA, Khiroug L, Hashimoto K, Hayasaka S, Oda SI, Inouye M, Takagishi Y, Augustine GJ, Kano M. Local calcium release in dendritic spines required for long-term synaptic depression. Neuron 2000;28:233-244.

Moraru II, Kaftan EJ, Ehrlich BE, Watras J. Regulation of type 1 inositol 1,4,5-trisphosphate-gated calcium channels by InsP3 and calcium: Simulation of single channel kinetics based on ligand binding and electrophysiological analysis. J.Gen.Physiol. 1999;113:837-849.

Othmer HG, Tang H. Oscillations and waves in a model of calcium dynamics. In: Othmer HG, Murray J and Maini P (eds), Experimental and Theoretical Advances in Biological Pattern Formation, Plenum Press, London, 1993, pp. 295-319.

Parys JB, Sernett SW, DeLisle S, Snyder PM, Welsh MJ, Campbell KP. Isolation, characterization, and localization of the inositol 1,4,5-trisphosphate receptor protein in Xenopus laevis oocytes. J.Biol.Chem. 1992;267:18776-18782.

Patel S, Joseph SK, Thomas AP. Molecular properties of inositol 1,4,5-trisphosphate receptors. Cell Calcium 1999;25:247-264.

Rizzuto R. Intracellular Ca(2+) pools in neuronal signalling. Curr.Opin.Neurobiol. 2001;11:306-311.

Sabatini BL, Maravall M, Svoboda K. Ca(2+) signaling in dendritic spines. Curr.Opin.Neurobiol. 2001;11:349-356.

Sabatini BL, Oertner TG, Svoboda K. The life cycle of Ca(2+) ions in dendritic spines. Neuron 2002;33:439-452.

Santamaria F, Wils S, De Schutter E, Augustine GJ. Anomalous diffusion in Purkinje cell dendrites caused by spines. Neuron 2006;52:635-648.

Schmidt H, Kunerth S, Wilms C, Strotmann R, Eilers J. Spino-dendritic crosstalk in rodent Purkinje neurons mediated by endogenous Ca2+-binding proteins. J.Physiol. 2007;

Sharp AH, Nucifora FC,Jr, Blondel O, Sheppard CA, Zhang C, Snyder SH, Russell JT, Ryugo DK, Ross CA. Differential cellular expression of isoforms of inositol 1,4,5-triphosphate receptors in neurons and glia in brain. J.Comp.Neurol. 1999;406:207-220.

Shuai JW, Jung P. Stochastic properties of Ca(2+) release of inositol 1,4,5-trisphosphate receptor clusters. Biophys.J. 2002;83:87-97.

Sneyd J, Dufour JF. A dynamic model of the type-2 inositol trisphosphate receptor. Proc.Natl.Acad.Sci.U.S.A. 2002;99:2398-2403.

Sneyd J, Falcke M. Models of the inositol trisphosphate receptor. Prog.Biophys.Mol.Biol. 2005;89:207-245.

Swillens S, Champeil P, Combettes L, Dupont G. Stochastic simulation of a single inositol 1,4,5-trisphosphate-sensitive Ca2+ channel reveals repetitive openings during 'blip-like' Ca2+ transients. Cell Calcium 1998;23:291-302.

Taylor CW, da Fonseca PC, Morris EP. IP(3) receptors: the search for structure. Trends Biochem.Sci. 2004;29:210-219.

Tu H, Wang Z, Bezprozvanny I. Modulation of mammalian inositol 1,4,5-trisphosphate receptor isoforms by calcium: a role of calcium sensor region. Biophys.J. 2005b;88:1056-1069.

Tu H, Wang Z, Nosyreva E, De Smedt H, Bezprozvanny I. Functional characterization of mammalian inositol 1,4,5-trisphosphate receptor isoforms. Biophys.J. 2005a;88:1046-1055.

Turner TE, Schnell S, Burrage K. Stochastic approaches for modelling in vivo reactions. Comput.Biol.Chem. 2004;28:165-178.

Wang SS, Denk W, Hausser M. Coincidence detection in single dendritic spines mediated by calcium release. Nat.Neurosci. 2000;3:1266-1273.

Wils S, De Schutter E. 3-dimentional stochastic simulation of biochemical pathways. Knowledge for growth: Annual Flemish Biotech Convention, Gent, Belgium, June 3rd, 2005.

Wils S, De Schutter E. STEPS: Stochastic simulation of reaction-diffusion in complex 3-D environment. 15th Annual Meeting of the Organization for Computational Neurosciences CNS*2006, Edinburgh, UK, July 16-20, 2006.

Yamamoto-Hino M, Sugiyama T, Hikichi K, Mattei MG, Hasegawa K, Sekine S, Sakurada K, Miyawaki A, Furuichi T, Hasegawa M. Cloning and characterization of human type 2 and type 3 inositol 1,4,5-trisphosphate receptors. Receptors Channels 1994;2:9-22.

Yao Y, Choi J, Parker I. Quantal puffs of intracellular Ca2+ evoked by inositol trisphosphate in Xenopus oocytes. J.Physiol. 1995;482:533-553.

Zumdahl SS. Chemical principles, Houghton Mifflin Company, Boston, New York, USA, 1998, pp. 192-193.

Appendix A: STEPSML

An example of STEPSML, specific XML based markup language used in STEPS. In this file the model of Doi et al. (2005) is described.

```
<?xml version="1.0" encoding="UTF-8"?>
<!-- Based on Doi 2005 -->
<!-- Volumes: cytosol 0.1 μM, ER 0.1 μM -->
<!-- Initial cytosolic concs: IP3 0.2 μM, Ca_cyt 0.10 μM -->
<!-- Resolution 0.4642e-6 -->

<stepsml>
   <model name="IP3R_Doi">

   <simulation name="default">
      <set-tstart>0.0</set-tstart>
      <set-tend>20.0</set-tend>
      <set-istart>0</set-istart>
      <set-iend>99</set-iend>
      <set-res>0.4642e-6</set-res>
      <set-rngseed>
           ( 13, 23, 24, 26, 50, 56, 82, 101, 145, 134, 157, 161, 223,
           276, 463, 537, 619, 835, 712, 953,
           1038, 1187, 1234, 1398, 1787, 1982, 2006, 2002, 2222, 3333,
           9876, 3572, 2938, 33873, 28374,
           109, 2875, 3, 9765, 24592, 2947, 8374, 65983, 1739, 45,
           9274, 27455, 45774, 4636, 1345,
           387, 357, 8542, 3639, 45253, 8475, 337, 432, 876, 5678,
           2345, 8436, 78586, 9838, 87,
           9756, 568, 456, 764, 66, 298, 887, 8475, 2387, 564, 907,
           2653, 8543, 375, 9364,
           6592, 2146, 965, 356, 2712, 444, 787, 888, 949, 549, 111,
           8888, 4433, 6677, 9988,
          343, 656, 878, 989, 4422 )
      </set-rngseed>
   </simulation>

      <species name="Ca"></species>
      <species name="IP3"></species>
      <species name="IP3R_RIC"></species>
      <species name="IP3R_RI"></species>
      <species name="IP3R_R"></species>
      <species name="IP3R_RC"></species>
      <species name="IP3R_RC2"></species>
      <species name="IP3R_RC3"></species>
      <species name="IP3R_RC4"></species>

      <volume name="cytosol">
      </volume>

      <compartment>
         <set-volume>cytosol</set-volume>

         <geometry>
            <box>
               <set-min>(-0.2321e-6, 0.0e-6, 0.0e-6)</set-min>
```

```
         <set-max>( 0.2321e-6, 0.4642e-6, 0.4642e-6)</set-max>
      </box>
   </geometry>
</compartment>

<volume name="ER">
</volume>

<compartment>
   <set-volume>ER</set-volume>
   <geometry>
      <box>
         <set-min>(-0.2321e-6, 0.4642e-6, 0.0e-6)</set-min>
         <set-max>( 0.2321e-6, 0.9284e-6, 0.4642e-6)</set-max>
      </box>
   </geometry>
</compartment>

<surface name="ER_CS">

   <set-in>ER</set-in>
   <set-out>cytosol</set-out>

   <!-- Flux through the open channel -->

   <inst-xstrans type="outflux_diff">
      <set-param name="x">Ca</set-param>
      <set-param name="r">IP3R_RIC</set-param>
      <set-param name="kf">5.8e8</set-param>
      <set-param name="clamp_x_in">false</set-param>
   </inst-xstrans>

   <!-- RI + Ca <=> RIC -->

   <inst-xstrans name="ri_ca___ric" type="bind_ligand_out">
      <set-param name="x">Ca</set-param>
      <set-param name="r">IP3R_RI</set-param>
      <set-param name="rx">IP3R_RIC</set-param>
      <set-param name="kf">8000e6</set-param>
   </inst-xstrans>

   <inst-xstrans name="ric___ri_ca" type="unbind_ligand_out">
      <set-param name="rx">IP3R_RIC</set-param>
      <set-param name="r">IP3R_RI</set-param>
      <set-param name="x">Ca</set-param>
      <set-param name="kf">2000</set-param>

   <!-- R + IP3 <=> RI -->

   </inst-xstrans>
      <inst-xstrans name="r_ip3___ri" type="bind_ligand_out">
      <set-param name="x">IP3</set-param>
      <set-param name="r">IP3R_R</set-param>
      <set-param name="rx">IP3R_RI</set-param>
      <set-param name="kf">1000e6</set-param>
   </inst-xstrans>

   <inst-xstrans name="ri___r_ip3" type="unbind_ligand_out">
      <set-param name="rx">IP3R_RI</set-param>
      <set-param name="r">IP3R_R</set-param>
      <set-param name="x">IP3</set-param>
```

```
   <set-param name="kf">25800</set-param>
</inst-xstrans>

<!-- R + Ca <=> RC -->

<inst-xstrans name="r_ca___rc" type="bind_ligand_out">
   <set-param name="x">Ca</set-param>
   <set-param name="r">IP3R_R</set-param>
   <set-param name="rx">IP3R_RC</set-param>
   <set-param name="kf">8.889e6</set-param>
</inst-xstrans>

<inst-xstrans name="rc___r_ca" type="unbind_ligand_out">
   <set-param name="rx">IP3R_RC</set-param>
   <set-param name="r">IP3R_R</set-param>
   <set-param name="x">Ca</set-param>
   <set-param name="kf">5</set-param>
</inst-xstrans>

<!-- RC + Ca <=> RC2 -->

<inst-xstrans name="rc_ca___rc2" type="bind_ligand_out">
   <set-param name="x">Ca</set-param>
   <set-param name="r">IP3R_RC</set-param>
   <set-param name="rx">IP3R_RC2</set-param>
   <set-param name="kf">20e6</set-param>
</inst-xstrans>

<inst-xstrans name="rc2___rc_ca" type="unbind_ligand_out">
   <set-param name="rx">IP3R_RC2</set-param>
   <set-param name="r">IP3R_RC</set-param>
   <set-param name="x">Ca</set-param>
   <set-param name="kf">10</set-param>
</inst-xstrans>

<!-- RC2 + Ca <=> RC3 -->

<inst-xstrans name="rc2_ca___rc3" type="bind_ligand_out">
   <set-param name="x">Ca</set-param>
   <set-param name="r">IP3R_RC2</set-param>
   <set-param name="rx">IP3R_RC3</set-param>
   <set-param name="kf">40e6</set-param>
</inst-xstrans>

<inst-xstrans name="rc3___rc2_ca" type="unbind_ligand_out">

   <set-param name="rx">IP3R_RC3</set-param>
   <set-param name="r">IP3R_RC2</set-param>
   <set-param name="x">Ca</set-param>
   <set-param name="kf">15</set-param>
</inst-xstrans>
```

```
   <!-- RC3 + Ca <=> RC4 -->

   <inst-xstrans name="rc3_ca___rc4" type="bind_ligand_out">
      <set-param name="x">Ca</set-param>
      <set-param name="r">IP3R_RC3</set-param>
      <set-param name="rx">IP3R_RC4</set-param>
      <set-param name="kf">60e6</set-param>
   </inst-xstrans>

   <inst-xstrans name="rc4___rc3_ca" type="unbind_ligand_out">
      <set-param name="rx">IP3R_RC4</set-param>
      <set-param name="r">IP3R_RC3</set-param>
      <set-param name="x">Ca</set-param>
      <set-param name="kf">20</set-param>
   </inst-xstrans>

</surface>

<!-- Initial values -->

<window>
   <add-volume>cytosol</add-volume>
   <geometry>
      <box>
         <set-min>(-0.2321e-6, 0.0e-6, 0.0e-6)</set-min>
         <set-max>( 0.2321e-6, 0.4642e-6, 0.4642e-6)</set-max>
      </box>
   </geometry>

   <inst-sourcesink type="inject_conc_volume">
      <set-param name="s">Ca</set-param>
      <set-param name="C">0.10e-6</set-param>
      <set-param name="ts">0.0</set-param>
      <set-param name="te">0.0</set-param>
      <set-param name="p">1e150</set-param>
   </inst-sourcesink>

   <inst-sourcesink type="inject_conc_volume">
      <set-param name="s">IP3</set-param>
      <set-param name="C">0.2e-6</set-param>
      <set-param name="ts">0.0</set-param>
      <set-param name="te">0.0</set-param>
      <set-param name="p">1e150</set-param>
   </inst-sourcesink>
</window>

<window>
   <add-volume>ER</add-volume>
   <geometry>
      <box>
         <set-min>(-0.2321e-6, 0.4642e-6, 0.0e-6)</set-min>
         <set-max>( 0.2321e-6, 0.9284e-6, 0.4642e-6)</set-max>
      </box>
   </geometry>

   <inst-sourcesink type="inject_conc_volume">
      <set-param name="s">Ca</set-param>
      <set-param name="C">150.0e-6</set-param>
      <set-param name="ts">0.0</set-param>
      <set-param name="te">0.0</set-param>
      <set-param name="p">1e150</set-param>
```

```
   </inst-sourcesink>
</window>

<window>
   <add-surface>ER_CS</add-surface>
   <geometry>
      <box>
         <set-min>(-0.2321e-6, 0.0e-6, 0.0e-6)</set-min>
         <set-max>( 0.2321e-6, 0.9284e-6, 0.4642e-6)</set-max>
      </box>
   </geometry>

   <inst-sourcesink type="inject_mass_surface">
      <set-param name="x">IP3R_R</set-param>
      <set-param name="n">16</set-param>
      <set-param name="ts">0.0</set-param>
      <set-param name="te">0.0</set-param>
      <set-param name="p">1e150</set-param>
   </inst-sourcesink>
</window>

<!-- Samplers -->

<window>
   <add-volume>cytosol</add-volume>
   <geometry>
      <box>
         <set-min>(-0.2321e-6, 0.0e-6, 0.0e-6)</set-min>
         <set-max>( 0.2321e-6, 0.4642e-6, 0.4642e-6)</set-max>
      </box>
   </geometry>

   <inst-sampler type="sample_mass">
      <set-param name="s">Ca</set-param>
      <set-param name="ts">0</set-param>
      <set-param name="te">0.5</set-param>
      <set-param name="p">1e-4</set-param>
      <set-param name="out">doi/dyn/010C/010C_cyto_ca
         </set-param>
   </inst-sampler>

   <inst-sampler type="sample_mass">
      <set-param name="s">IP3</set-param>
      <set-param name="ts">0.0</set-param>
      <set-param name="te">0.5</set-param>
      <set-param name="p">1e-4</set-param>
      <set-param name="out">doi/dyn/010C/010C_cyto_ip3
         </set-param>
   </inst-sampler>
</window>

<window>
   <add-surface>ER_CS</add-surface>
   <geometry>
      <box>
         <set-min>(-0.2321e-6, 0.0e-6, 0.0e-6)</set-min>
         <set-max>( 0.2321e-6, 0.9284e-6, 0.4642e-6)</set-max>
      </box>
   </geometry>

   <inst-sampler type="sample_mass">
```

```
            <set-param name="s">IP3R_RIC</set-param>
            <set-param name="ts">0.0</set-param>
            <set-param name="te">0.5</set-param>
            <set-param name="p">1e-4</set-param>
            <set-param na me="out">doi/dyn/010C/010C_membr_ric
               </set-param>
         </inst-sampler>
      </window>

   </model>
</stepsml>
```